~~CONFIDENTIAL~~

CALIFORNIA INSTITUTE OF TECHNOLOGY

Hydrodynamics Laboratories

CAVITY FLOW DRAG ON SPINNING PROJECTILES

A REPORT ON RESEARCH CONDUCTED UNDER CONTRACT WITH
THE BUREAU OF ORDNANCE OF THE DEPARTMENT OF THE NAVY

~~CONFIDENTIAL~~

~~CONFIDENTIAL~~

Navy Department

Bureau of Ordnance Contract NOrd 9612

CAVITY FLOW DRAG ON SPINNING PROJECTILES

by

JOHN KAYE
Research Engineer

HYDRODYNAMICS LABORATORY
California Institute of Technology
Pasadena, California
Robert T. Knapp, Director

September, 1949 Report No. N-50

Copy No. 140

~~CONFIDENTIAL~~

CONTENTS

ABSTRACT

Measurements were made of the drag forces acting on projectile noses rotating at zero yaw about an axis parallel to the direction of the approaching flow. The noses were rotating in the cavity formed at a cavitation number of about 0.29, based upon the approach velocity. Thus, only the front portion of the nose was in contact with the water.

Hemisphere

Within the limited range of tests made, the drag on a hemispherical nose decreased with an increase in the rotational speed at a constant stream velocity. The magnitude of this drop in drag was essentially independent of the stream velocity. At any stream velocity the difference between the drag at a given rotative speed and the drag at zero rotative speed was approximately equal to the corresponding difference at any other stream velocity.

The drag coefficient was the same function of the ratio of rotative velocity to stream velocity for all conditions.

Changes in flow conditions at the nose were sufficiently great to be observed visually. The sharp ring of separation of the flow at the nose when there was no rotation became a somewhat ragged zone of separation at the higher rotative speeds.

The nose was a 2-3/8 in. diameter hemisphere mounted on a short section of circular cylinder. Stream velocities of 30, 39, and 55 ft per sec were used. Rotative speeds ranged from zero to 7200 rpm. This corresponds to linear peripheral velocities from zero to 75 ft per sec based upon the 2-3/8-in. diameter.

Truncated Cone

Measurements were also made of the drag forces acting on a truncated cone whose upstream face was of 1-1/4-in. diameter. This cone acted essentially as a disk since the cavity formed at the edge of the upstream face. The drag force was constant at each value of stream velocity independent of rotative speed. Tests were made at stream velocities of 39 and 50 ft per sec with rotative speeds ranging from zero to 7200 rpm.

Analysis

Some of the considerations contributing to the observed behavior are indicated but no complete explanation has been developed.

GENERAL

Interest in the underwater behavior of spin stabilized projectiles was greatly stimulated when tests demonstrated that specific head designs would produce stable underwater trajectories. Later work was directed toward developing a low drag shape which would still give a stable trajectory. In all of the reported investigations the test projectile was fired from a standard rifled gun into an open tank. The trajectories were recorded and the drag data were obtained from these.

In order to predict the behavior of projectiles, it is necessary to understand the forces which act upon them and to know the magnitudes of these forces. Spin stabilized projectiles which are used in underwater warfare will, in general, have entered from the air. Their performance will depend significantly upon the forces which act at water entry and in the subsequent cavity stage.

The characteristics of flow about nonrotating bodies under cavitation conditions have been studied.[1,2]* However, no corresponding information is available for spinning projectiles. Apparently the only laboratory investigations of bodies rotating about an axis parallel to the flow were made in air.[3,4] Such force data are not applicable to cavitation conditions. Thus, there is need for fundamental studies of the forces on spinning shapes in cavitation bubbles.

PURPOSE

This investigation was undertaken to determine the forces acting on bodies spinning in cavitation bubbles, and to observe the behavior of the flow. It was limited to the case of bodies spinning at zero yaw about an axis parallel to the flow. Although the intent was to measure both the axial drag force and the spin decelerating moment, this report concerns itself only with the drag force.

TEST CONDITIONS

Apparatus

The investigation was made in the High Speed Water Tunnel.[5] This is a closed circuit unit, providing for control and measurement of stream velocity, working section pressure, and temperature. It is equipped with a 14-in. diameter closed working section with lucite windows. The water tunnel balance measures three components: the drag in the direction of flow, the cross force perpendicular to the direction of flow, and the horizontal moment about the support point. The balance consists of a vertical spindle supported by a wire suspension system. The test object is mounted at the top of the spindle. Hydraulic systems apply forces to the lower end of the spindle in the drag and cross force directions. These forces are measured by precision gages. A similar system measures the moment about the support point. A schematic representation of the force measuring system is presented in Fig. 1.

A strobotac was used to measure rotating speed in conjunction with a thin dye stripe on the test nose.

* See bibliography at end of this report

Photographs were taken with a modified Fairchild K-17 camera. Illumination was provided by Edgerton-type flash lamps with flash duration of about 50 microseconds.

Test Unit

The test unit consisted of a nose shape mounted on the shaft of a compact 3-phase, 2-pole induction motor. The motor was rigidly attached to a spindle which was, in turn, firmly mounted on the balance spindle. Power was supplied from a variable frequency source by wires in the spindle. A sectional view of the motor cartridge is given in Fig. 2.

The motor cartridge and model spindle were shielded from the flow. Only the forward section of the nose was in contact with the water under cavitation conditions. The arrangement of elements is shown diagrammatically in Fig. 3. A view of the nose, motor, and model spindle is presented as Fig. 4. This unit was mounted rigidly on the balance spindle. Figs. 5 and 6 are photographs of the shielding unit which prevented hydrodynamic forces other than those acting on the nose from being transmitted to the balance under cavitation conditions. The assembly of the test and shielding units is seen in Fig. 7. Adequate clearance was left between the two units to prevent contact and interference.

The test unit was mounted with its axis parallel to the tunnel axis except for a slight nose-up pitch of one minute. This was tolerated because of the mechanical requirements of the assembly. Some yaw and pitch were allowed in the shielding unit since it was believed that no significant interference with the flow at the nose would occur. The spindle shield was yawed about four minutes, counterclockwise looking down. The model shield was pitched nose down about seven minutes.

The motor cartridge was filled with oil at the beginning of each daily period of test work. This was done to help dissipate heat and to protect the windings by keeping out the water during noncavitation conditions. However, oil seeped out and water entered through the bearings. Consequently the insulation broke down, forcing termination of the program.

Test Shapes

From the general principles of the ballistics of underwater projectiles, it is known that nose forces, such as found in cavity flow, are destabilizing on all shapes except blunt ones. As the rough limits of blunt noses, one can take a disk and a hemisphere. Additionally, the hemisphere is an interesting shape because much work has been done on hemispheres and spheres under various hydrodynamic conditions. Therefore, a hemisphere and a truncated cone were selected for the experiment.

An outline of the hemispherical nose is shown in Fig. 8. It will be noted that it consists of hemispherical and cylindrical portions. An outline of the truncated cone nose is presented in Fig. 9. The 2-3/8-in. maximum diameter of these noses was larger than the 2-in. diameter normally used. This was made necessary by the size of the motor cartridge and shield. The outside diameter of the upstream lip of the motor shield was 1/8-in. less than the nose diameter. The diameter of the upstream face of the truncated cone was determined from consideration of the capacity of the balance and the size of bubble expected. The noses were made of stainless steel and polished.

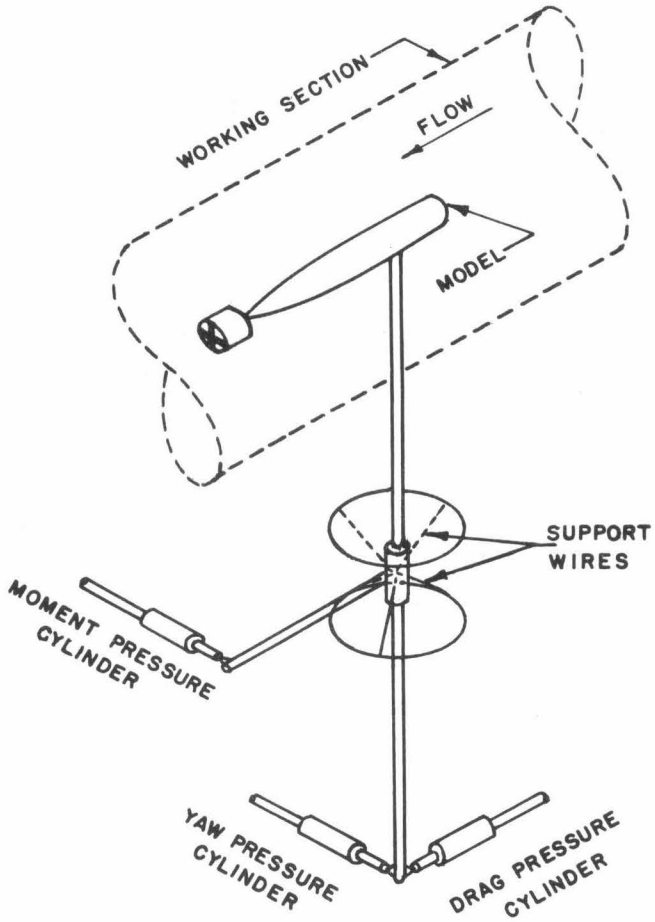

Fig. 1 - Diagrammatic Representation of Force Measuring System

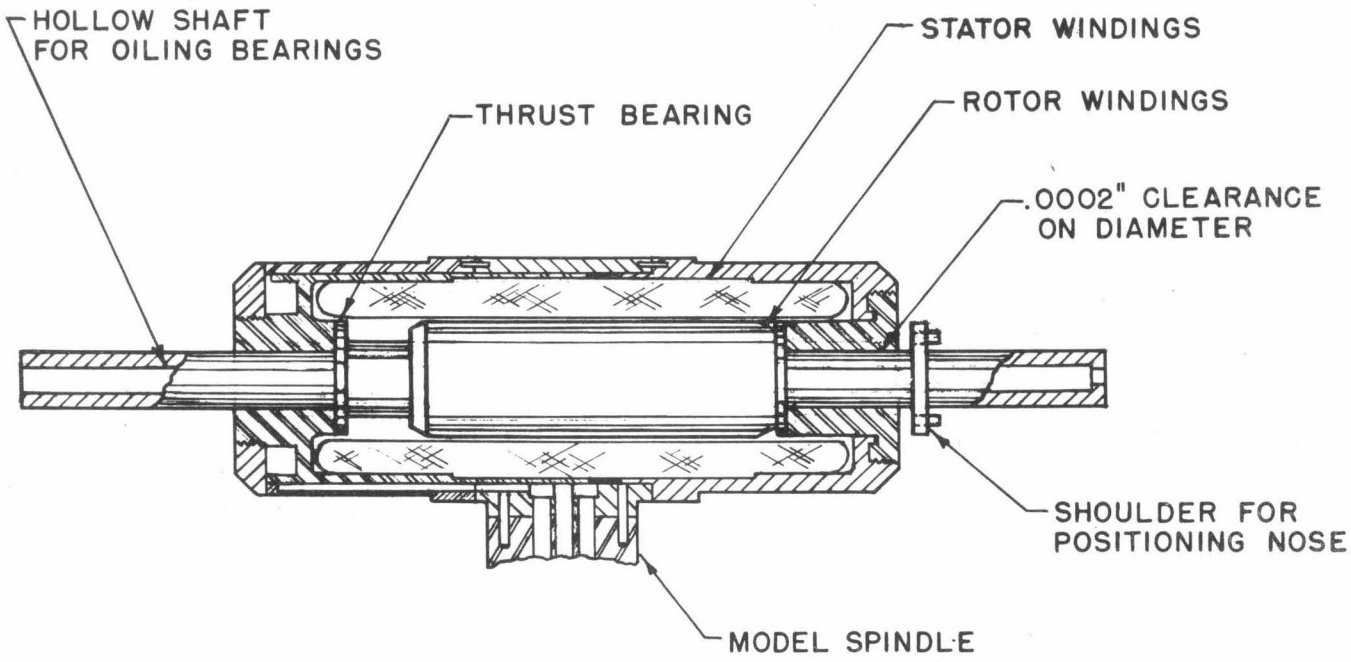

Fig. 2 - Section through Motor Cartridge

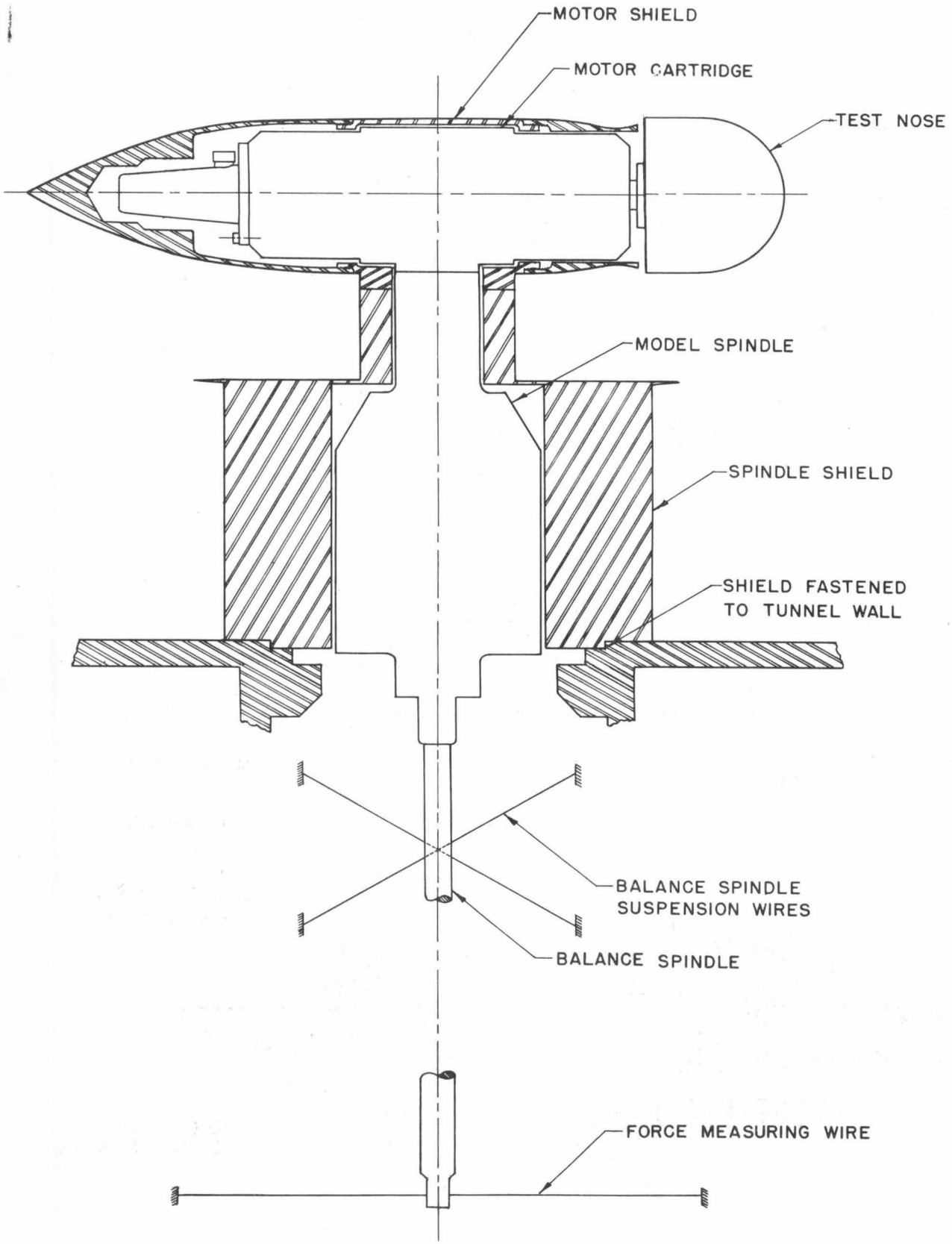

Fig. 3 - Outline of Test Unit, Spindles, and Shielding

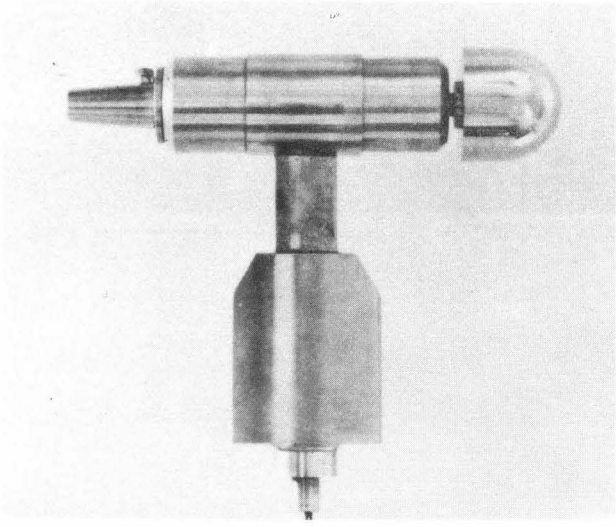

Fig. 4 - Hemispherical Nose Mounted on Shaft of Motor which is Rigidly Attached to Model Spindle

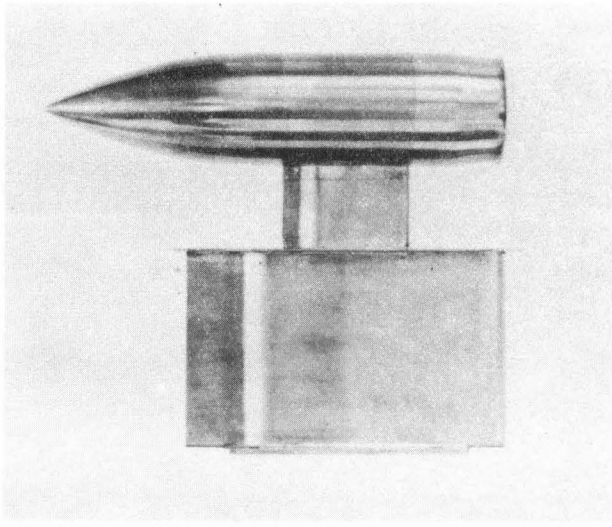

Fig. 5 - Shield for Motor and Spindle

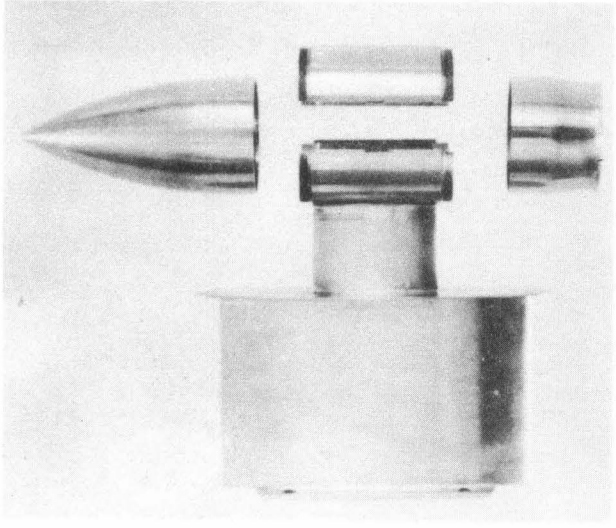

Fig. 6 - Exploded View of Shield for Motor and Spindle

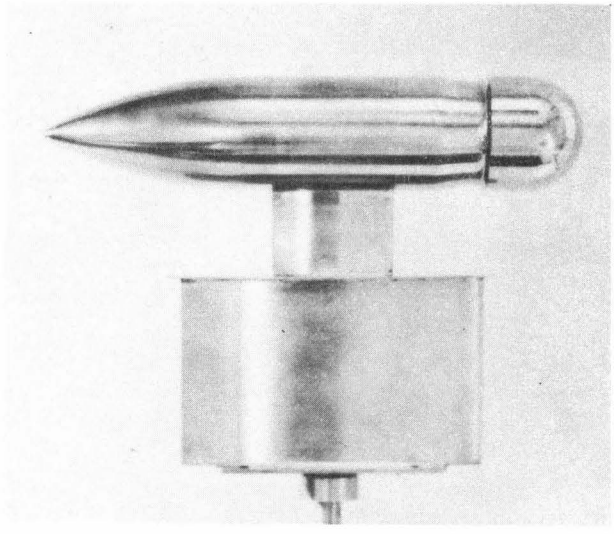

Fig. 7 - View of Rotating Projectile and Shield Assembly

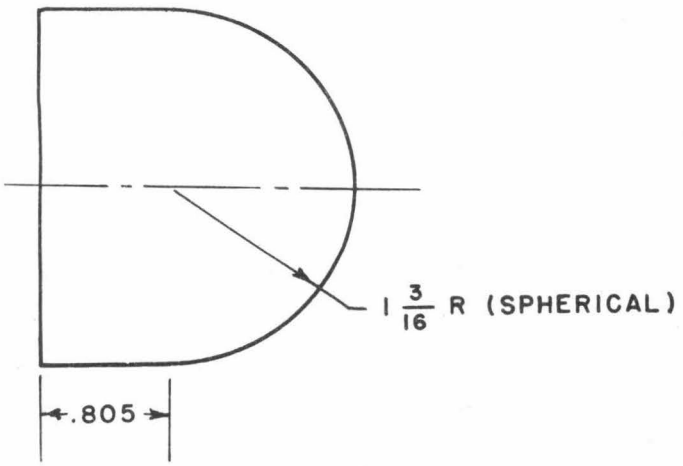

Fig. 8 - Outline of Hemispherical Nose

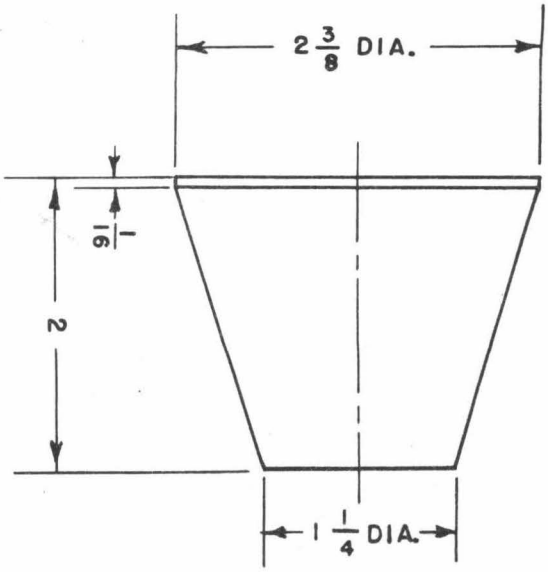

Fig. 9 - Outline of Truncated Cone Nose

EXPERIMENTS

General

In order to obtain meaningful information, it was decided to take all data at a constant value of the cavitation parameter,

$$K = \frac{p - p_v}{\rho \frac{v^2}{2}},$$

in which, for any consistent system of units,

K = dimensionless cavitation number

p = pressure in undisturbed flow in working section

p_v = water vapor pressure at temperature of cavity

ρ = mass densitv of water

V = velocity of undisturbed flow in working section

The nominal value of the cavitation number was selected as 0.29 since this produced a bubble large enough to clear the remaining portion of the nose and most of the motor shield. In this manner the forward portion of the nose was the only part of the spindle-supported unit which was subjected to hydrodynamic forces. The actual values of the cavitation parameter differed somewhat from the selected nominal value in the direction of a larger bubble in order to obtain stable conditions.

Hemispherical Nose

Measurements were made with the hemispherical nose at stream velocities of 30, 39, and 55 ft per sec. At 39 and 55 ft per sec data were obtained for both directions of rotation. Only one direction of rotation was used at 30 ft per sec. Rotative speeds of from zero to 7200 rpm were used. This corresponds to rotative linear velocities from zero to 75 ft per sec based upon the maximum diameter.

Truncated Cone Nose

Measurements were made at stream velocities of 39 and 50 ft per sec in both directions of rotation. Rotative speeds from zero to 7200 rpm were used.

RESULTS

Truncated Cone Nose

The data on drag force vs. rotative speed are presented as Fig. 10. It is seen that the drag force at a given approach velocity is independent of the speed of rotation of the nose. The data are consistent from the standpoint that the measurements for both directions of rotation fall on the same curves. The drag force is 13.2 lbs at 39 ft per sec and 21.1 lbs at 50 ft per sec.

The nose was enclosed in a clear, glassy bubble, similar to that shown in Fig. 11 for a square-end cylinder. Rotation did not produce any observable change in the bubble. Other aspects of the investigation indicate that no appreciable energy of rotation was introduced into the water by this nose.

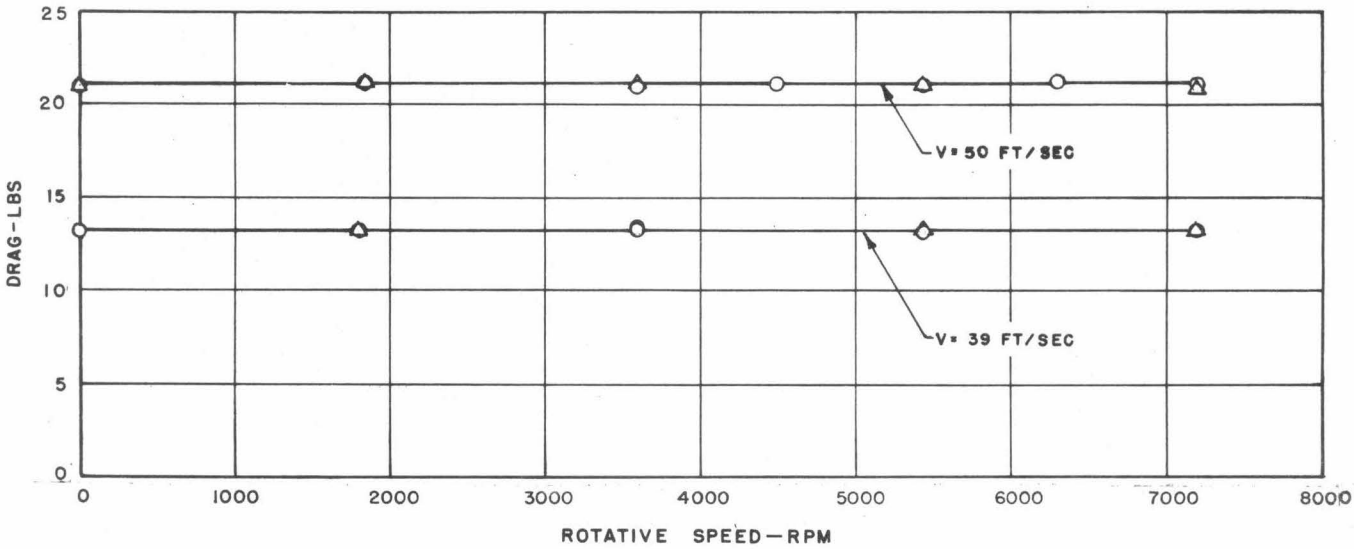

Fig. 10 - Drag vs. Rotative Speed for Truncated Cone Nose at K = 0.26

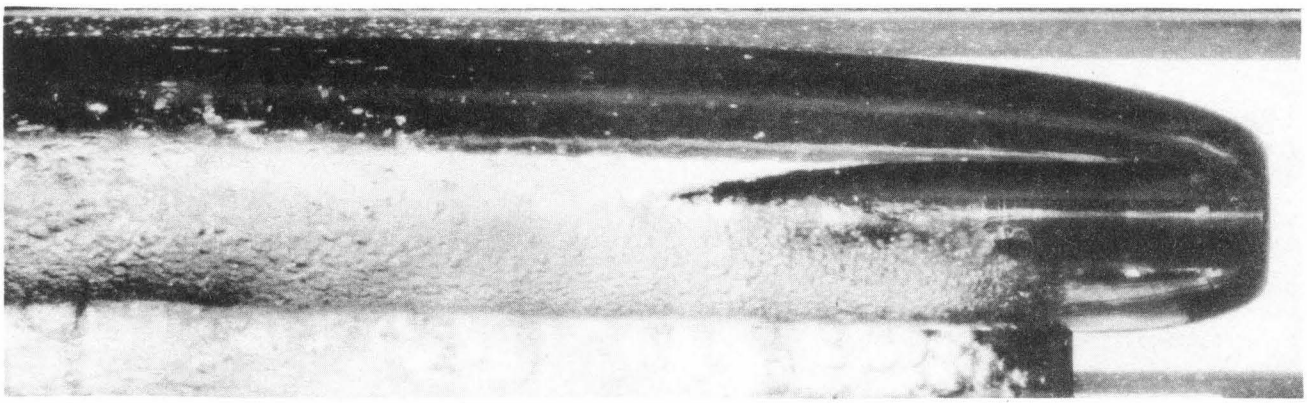

Fig. 11 - Clear, Glassy Bubble Produced by Square End Cylinder

Using the expression

$D = C_D A \frac{\rho}{2} V^2$, in which in any consistent system of units,

D = drag force

C_D = dimensionless drag coefficient

A = area based upon diameter of selected cross section

ρ = mass density

V = velocity of the undisturbed stream

Let

$(C_D)_1$ = drag coefficient when A is based upon the maximum diameter of the nose

$(C_D)_2$ = drag coefficient when A is based upon the area of the upstream face of the nose

Using the average experimental values of velocity,

at V = 39.2 ft per sec, $(C_D)_1 = 0.29$, $(C_D)_2 = 1.04$

V = 49.5 ft per sec, $(C_D)_1 = 0.29$, $(C_D)_2 = 1.04$

Since the measurements were made at the same value of the cavitation parameter, 0.26, it was expected that the coefficients based upon given areas would be independent of the stream velocity.

This nose acted as a circular disk of the diameter of its upstream face since the flow left the body at the edge of the face. It has been shown[6] from theoretical considerations that the drag coefficient of a body in a cavity can be evaluated approximately from knowledge of the drag coefficient at zero cavitation number and the cavitation number at test conditions. Thus

$$C_D = (C_D)_o (1 + K)$$

in which C_D = drag coefficient at cavitation number K, $(C_D)_O$ = drag coefficient when K = 0. For a circular disk, a theoretically determined value of 0.805 has been presented[7] for $(C_D)_O$. An experimentally determined value of 0.79 is presented in reference 6. Using the theoretical expression and the experimental value of 0.79 for $(C_D)_O$, C_D is calculated as 1.05 to compare with the measured values of 1.04.

Hemispherical Nose

Drag force vs. rpm curves for the hemispherical nose are presented as Fig. 12. The striking fact in these curves is that the drag force drops as the rotative speed is increased. Although the data scatter somewhat, there is an unmistakable decrease in the drag force with increase in rotative speed. The data for both directions of rotation at each of the velocities of 39 and 55 ft per sec define essentially the same curves. Data for only one direction of rotation were obtained at 30 ft per sec.

When the drag data for the three velocities are compared by superposing the maximum drag points, at zero rpm, it is seen that the change in drag is a function only of the rotative speed and not of the tunnel velocity. This is shown in Fig. 13.

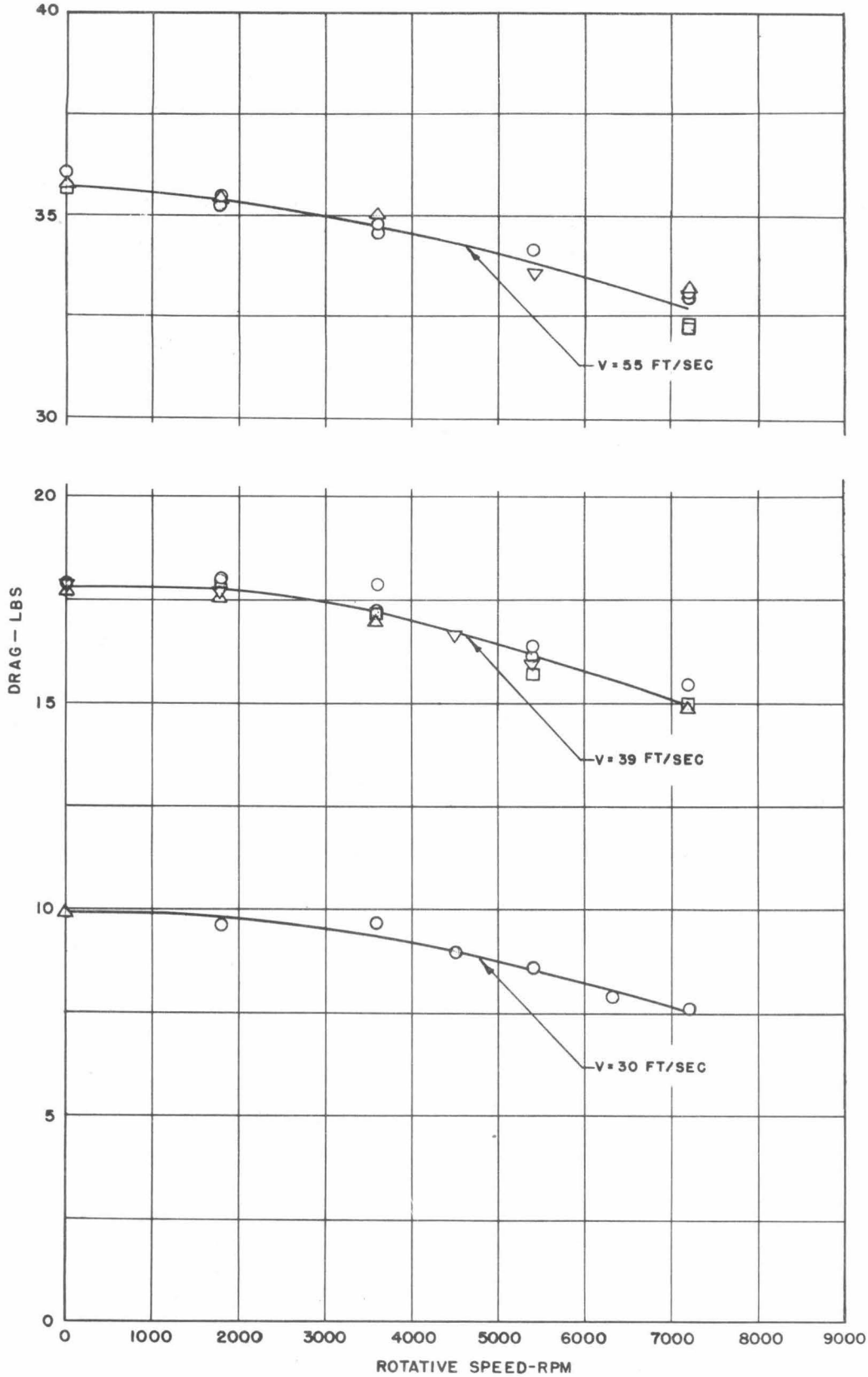

Fig. 12 - Hemispherical Nose
Rotation Decreases the Drag Force

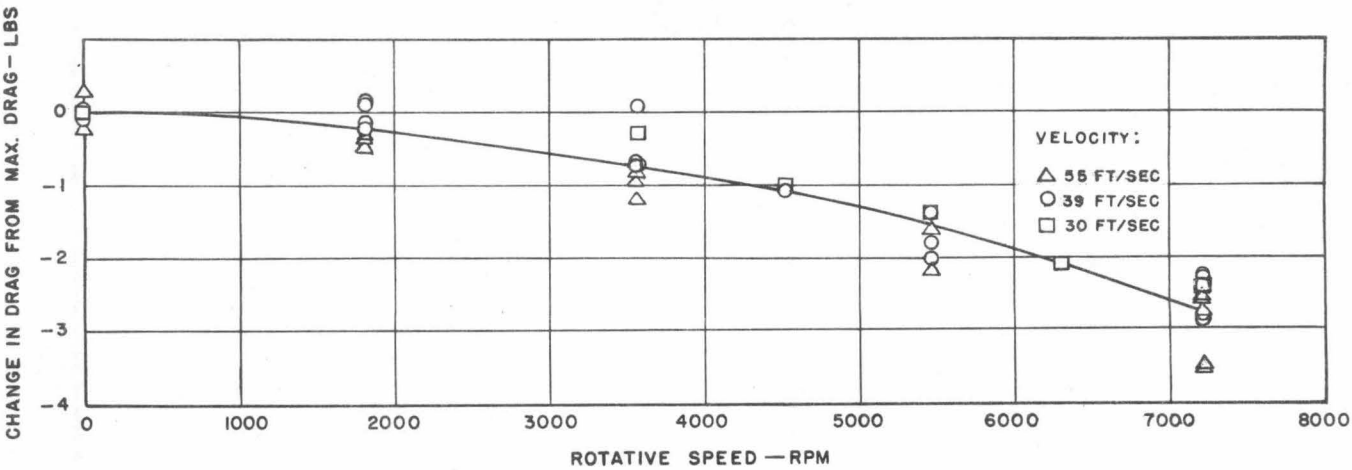

Fig. 13 - Hemispherical Nose

Change in Drag Caused by Rotation is Independent of Stream Velocity

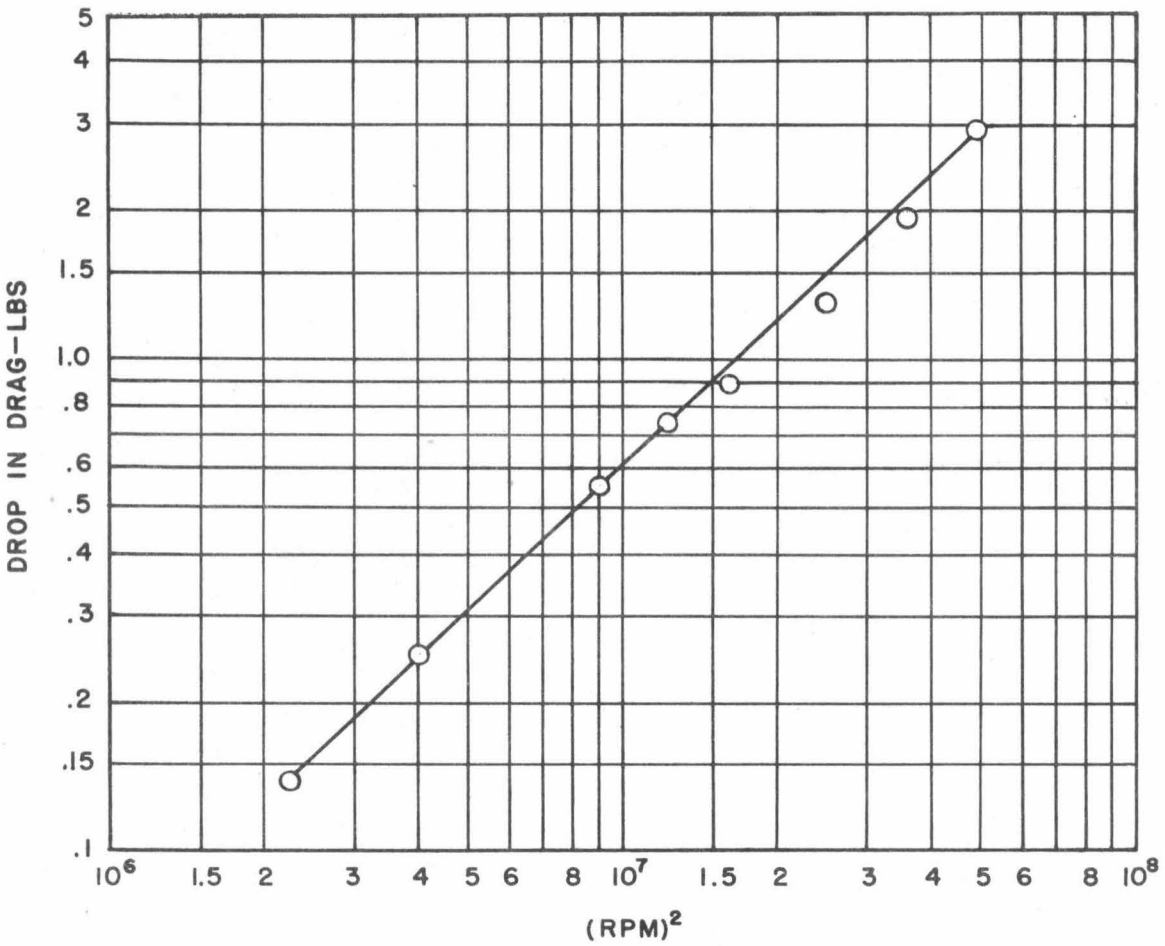

Fig. 14 - Hemispherical Nose

Drop in Drag Caused by Rotation is Proportional Approximately to the Square of the Rotative Speed

As a first approximation, the change in drag is proportional to the square of the rotative speed. This is deduced from Fig. 14 in which the log of the decrease in drag is plotted against the log of the square of the rotative speed. The points shown correspond to values represented by the curve of Fig. 13.

These results indicate that rotation is causing modification of the flow at the nose. The change in flow pattern may be observed visually as seen in Figs. 15 through 17. It will be noted that the photographs are presented in order of increase of the ratio ω/V of rotative speed to stream velocity. That the ratio ω/V is an important flow parameter will be shown later, and can be seen from the photographs. At low values of this parameter, the flow separated along a relatively regular line. As its value increased, the line of separation became irregular and, finally, jagged. The flow, which originally separated at one latitude, now separated over a range of latitudes. In fact, the aft separation point moved off the hemisphere onto the cylinder in some instances. The separation pattern remained fixed with respect to the nose for each condition.

Since the drag is a function of both the approach velocity and the rotative speed, the definition of a drag coefficient for the case of rotation should include the two factors. Furthermore, it should be rational in being determinate when either velocity goes to zero. Such a coefficient is obtained by making the drag a function of the square of an absolute velocity whose components are the undisturbed stream velocity and the peripheral velocity at the section of maximum diameter. Thus we have the expression

$$D = C_D \frac{\rho}{2} A_D (V^2 + r^2\omega^2)$$ in which, in any consistent system of units,

D = drag force

C_D = dimensionless coefficient of drag

ρ = mass density of the liquid

A_D = area based upon the diameter at the maximum cross section of object

V = velocity of the undisturbed flow in the working section

r = radius at maximum cross section of object

ω = rotational speed, radians per unit time

When this drag coefficient is calculated and values for all conditions of approach velocity and rotative speed are plotted against the ratio of the rotative speed to approach velocity in terms of ω/V, the points define a smooth curve, except for $\omega/V = 0$. That curve is presented as Fig. 18. The drag coefficient at zero rpm shows a slight dependence upon velocity. Other experimental data[1,8] indicate a value of C_D of 0.39 at a cavitation number of 0.30 without rotation.

It is to be remembered that the values of C_D obtained in this investigation refer not to a simple hemisphere, but to a hemisphere on a cylinder, in view of the fact that some of the flow was separating along the cylinder at the higher rotative speeds.

At the speeds of 39 and 55 ft per sec, most of the values of the cavitation number were either 0.30 or 0.29, with a few at 0.27 and 0.26. Conditions at 30 ft

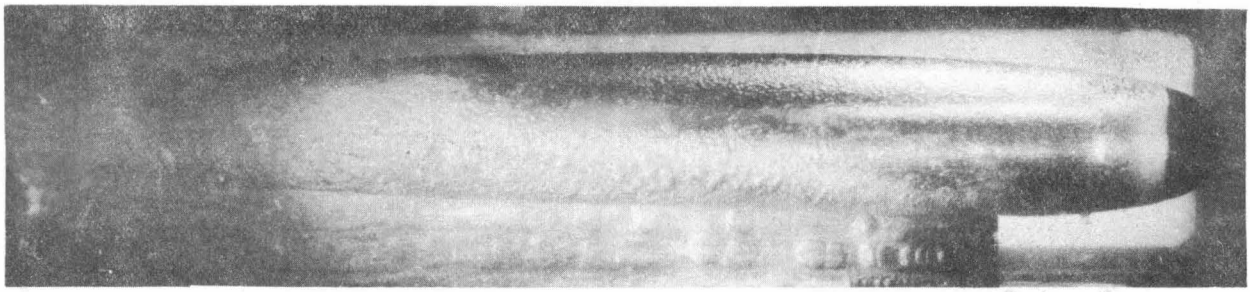

ω /V = 0 V = 55 FPS N = 0 RPM

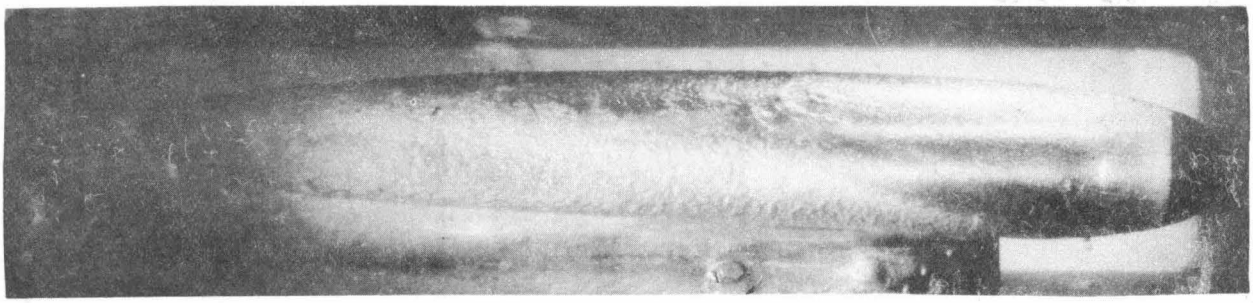

ω/V = 3.4 V = 55 FPS N = 1800 RPM

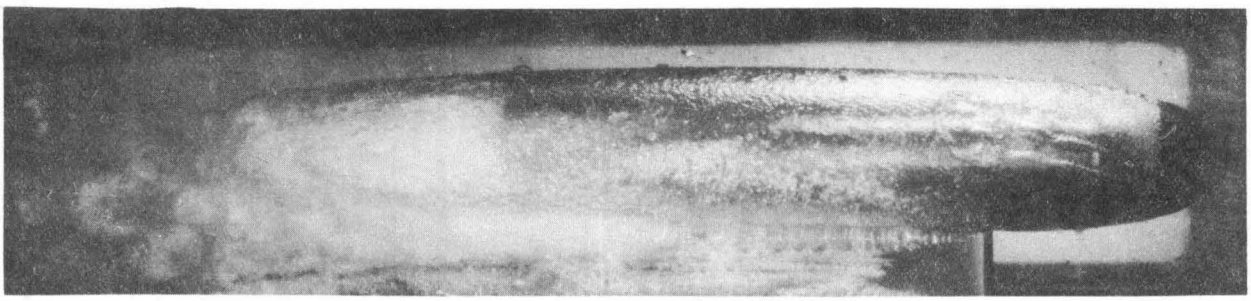

ω/V = 4.8 V = 39 FPS N = 1800 RPM

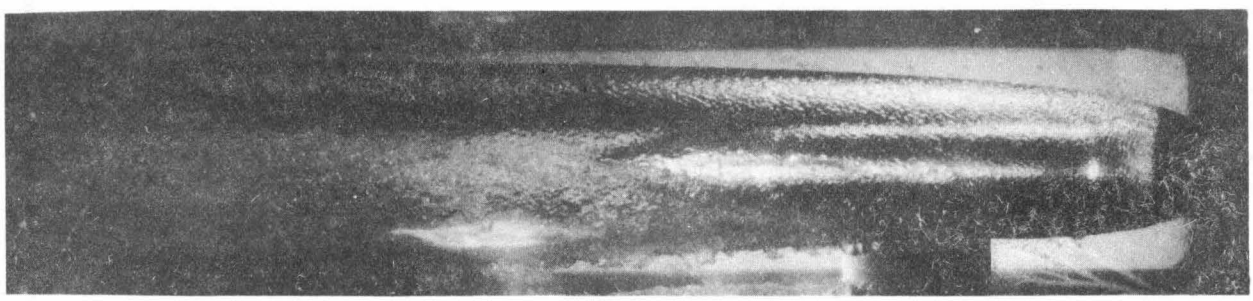

ω/V = 6.3 V = 30 FPS N = 1800 RPM

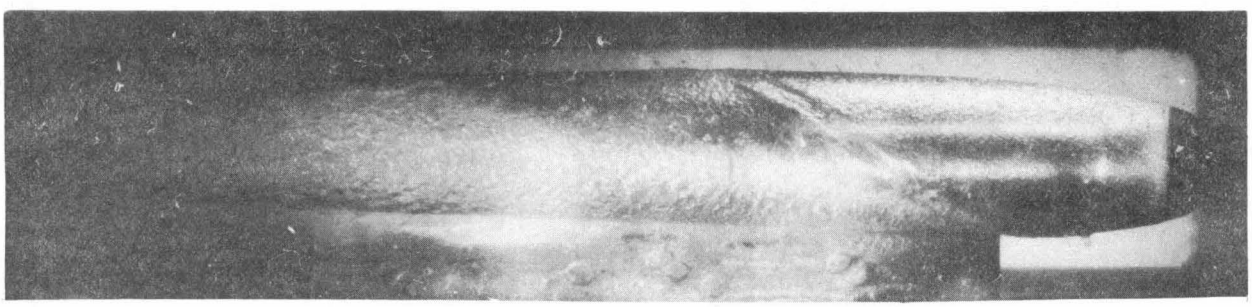

ω/V = 6.9 V = 55 FPS N = 3600 RPM

Fig. 15 - Flow Behavior is a Function of the Ratio ω/V of Rotative Speed to Stream Velocity

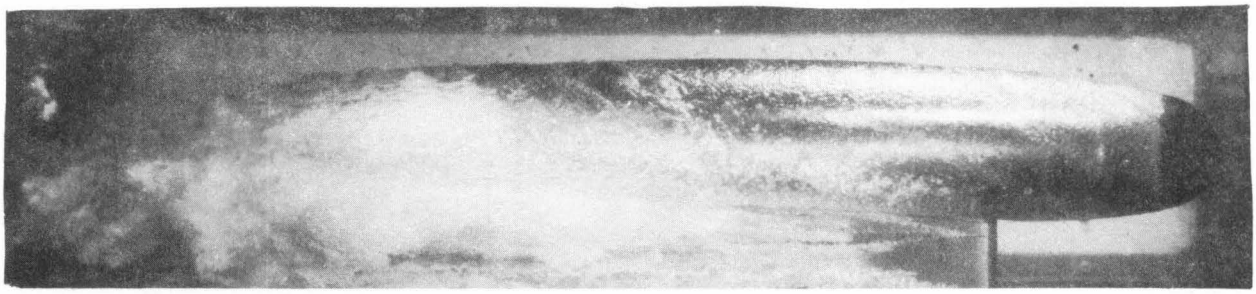

ω/V = 9.7 V = 39 FPS N = 3600 RPM

ω/V = 10.3 V = 55 FPS N = 5400 RPM

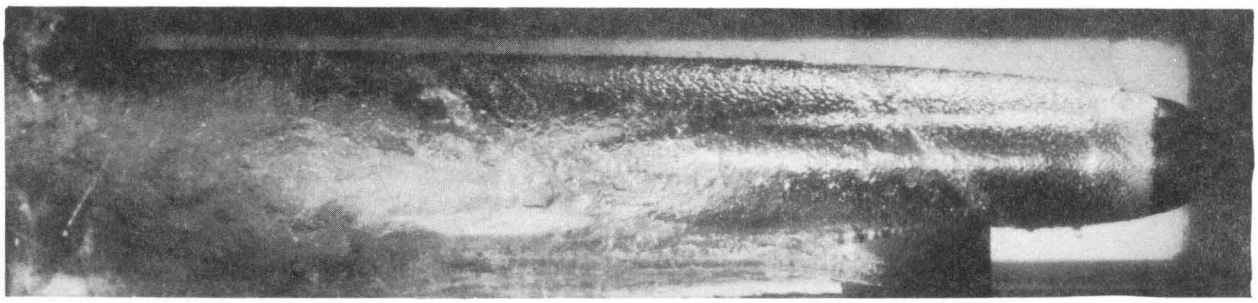

ω/V = 12.6 V = 30 FPS N = 3600 RPM

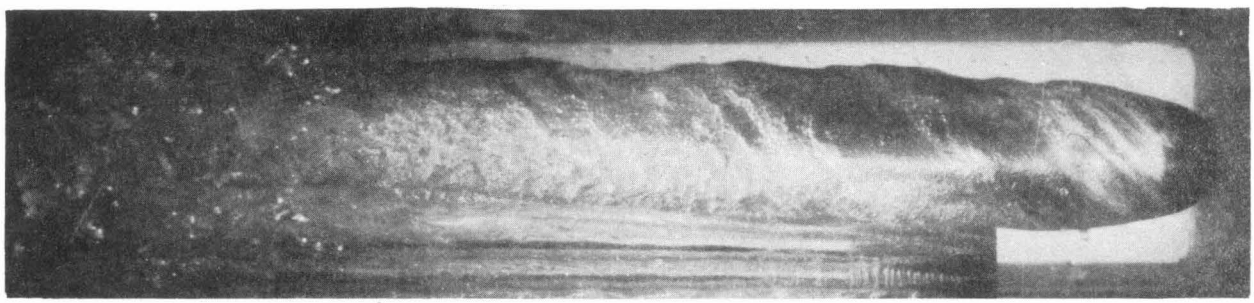

ω/V = 13.7 V = 55 FPS N = 7200 RPM

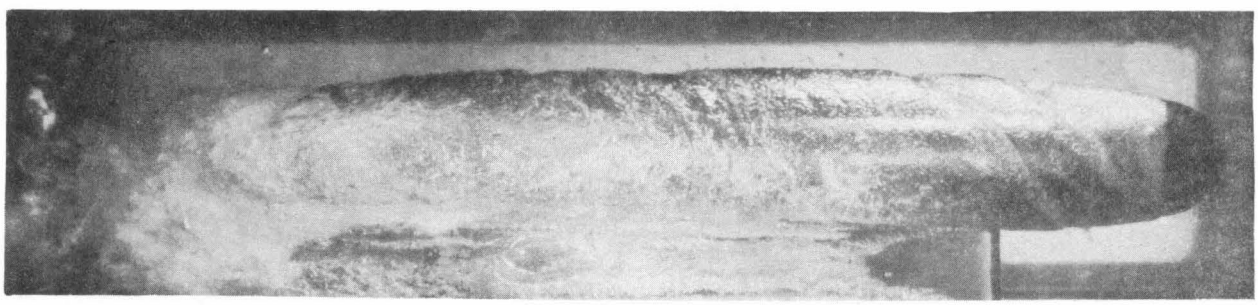

ω/V = 14.5 V = 39 FPS N = 5400 RPM

Fig. 16 - Flow Behavior is a Function of the Ratio ω/V of Rotative Speed to Stream Velocity

ω/V = 15.7 V = 30 FPS N = 4500 RPM

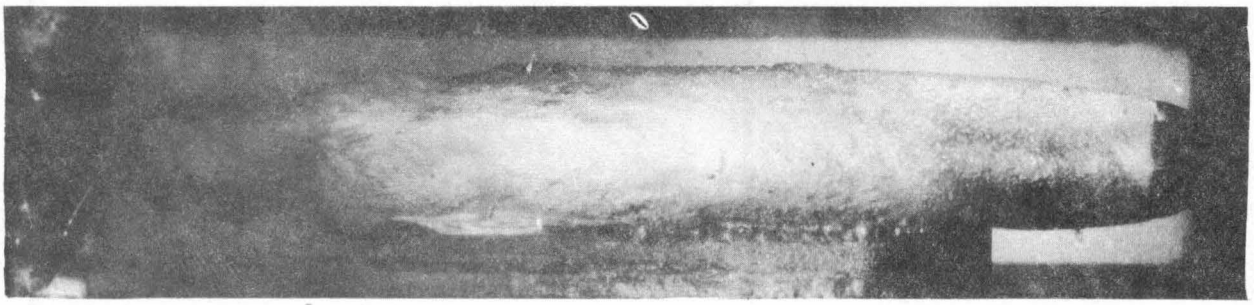

ω/V = 18.8 V = 30 FPS N = 5400 RPM

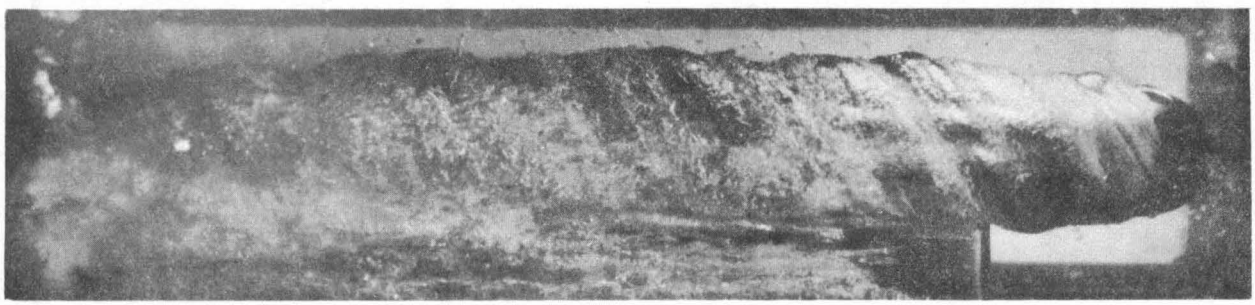

ω/V = 19.3 V = 39 FPS N = 7200 RPM

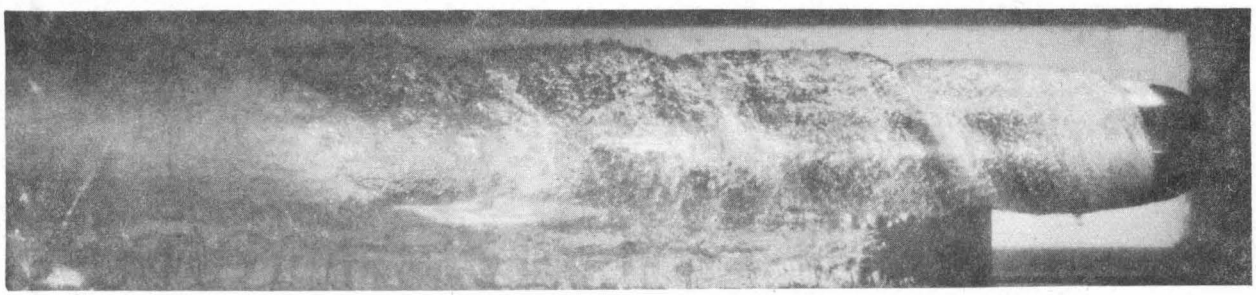

ω/V = 22.0 V = 30 FPS N = 6300 RPM

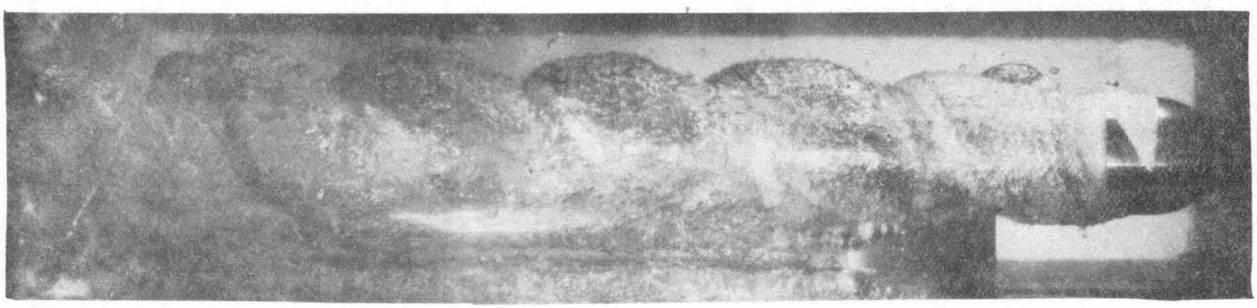

ω/V = 25.1 V = 30 FPS N = 7200 RPM

Fig. 17 - Flow Behavior is a Function of the Ratio ω/V of Rotative Speed to Stream Velocity

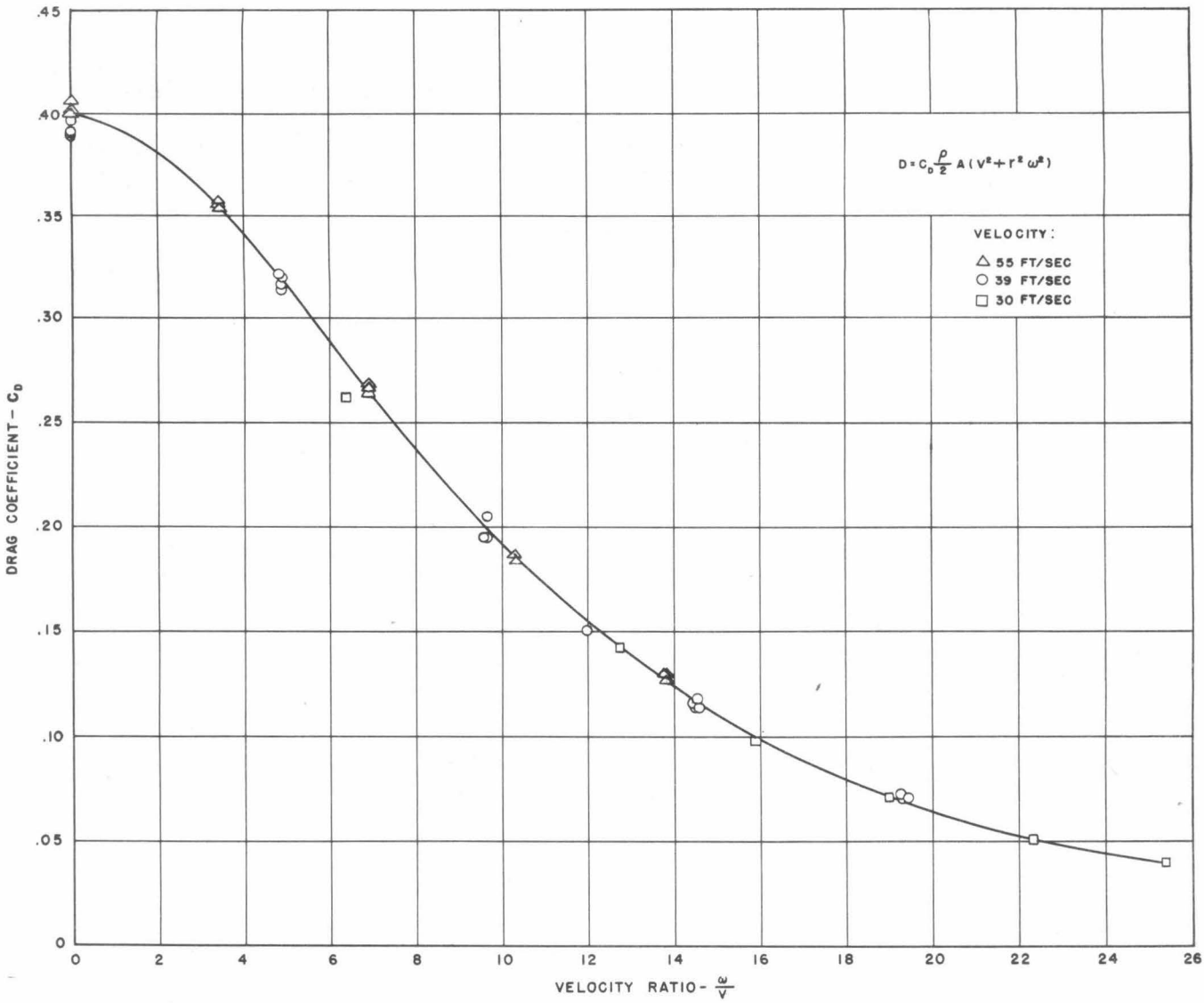

Fig. 18 - Hemispherical Nose

The Drag Coefficient is a Function of the Ratio of Rotative Speed to Stream Velocity

per sec were less stable. Most of the values of the parameter ranged from 0.30 to 0.28. Detailed information on the cavitation numbers and the drag force is presented in Appendix I.

The modification of the flow pattern at the nose shown in various of the photographs of Figs 15 through 17 is a phenomenon which appears to be associated with the type of flow condition. Wayland[9] has been studying the behavior of spinning spheres dropped into water. He has observed modification of the line of separation similar to that seen in the photographs. Associating this with the Reynolds number of the flow, he went to high Reynolds numbers without spin. He found that the separation point occurred ahead of the equator. However, when roughness was added to the nose, simulating an even higher Reynolds number, the region of separation moved aft of the nose. This condition seems to be similar to the transition from a laminar to a turbulent boundary layer in the case of a sphere in air.

Following this lead, the hemispherical nose was again mounted in a stationary condition in the tunnel but off the balance and unshielded. At a constant cavitation number and to the maximum velocity used, 85 ft per sec, no obvious changes in the bubble occurred. Artificial roughness was not added.

ANALYSIS

No theoretical analysis appears to have been made of the flow surrounding bodies rotating about an axis parallel to an approaching stream. Although no solution of that problem is presented, some of the factors influencing the flow are considered and an indication is made of the nature of the effect each may be expected to produce.

In cavity flow about a nonrotating object, the drag force is the resultant of the pressure forces and is influenced only slightly by viscous forces. This is seen from the fact that theoretical analyses, such as reported in reference 7, can make relatively accurate estimates of this force even though they assume an inviscid fluid. Pressure distributions obtained experimentally correspond closely to theoretical ones calculated for an ideal fluid for the forward portion of the body, the only portion in contact with the fluid under cavity conditions.

When the behavior of the flow about a body rotating in a cavity is considered, the effects of viscosity must be taken into account. This readily follows from the fact that a body rotating about an axis parallel to the approach direction of an ideal, frictionless fluid could put no energy into the fluid for lack of a mechanism of energy transfer. However, observation readily shows that energy of rotation is imparted to a real fluid. In particular, the experimental work being reported indicates very significant effects upon the flow produced by rotation of the body. With a hemisphere, a drop in drag, which is a function of the rotative speed, is found. Visual observation indicates important changes in the area of contact of fluid and body. The drag coefficient is a function of the ratio of the rotative speed to the velocity of the undisturbed flow. On the other hand, neither of these effects is observed when a disk is rotated in cavity flow. For simplicity, consider a uniform flow at velocity, v, of a fluid over a thin flat plate of finite width but infinite length which itself has a velocity, u, normal to that of the fluid, as seen in Fig. 19. A boundary layer will exist in the direction of the relative velocity, at an angle with the x-direction of

$$\alpha = \tan^{-1}\left(-\frac{v}{u}\right)$$

The resultant shear force will be a function of conditions in the boundary layer and will be in the direction of the relative velocity. The components of shear force in the x- and y-directions will depend upon the boundary layer conditions and be a function of the angle α or the ratio v/u.

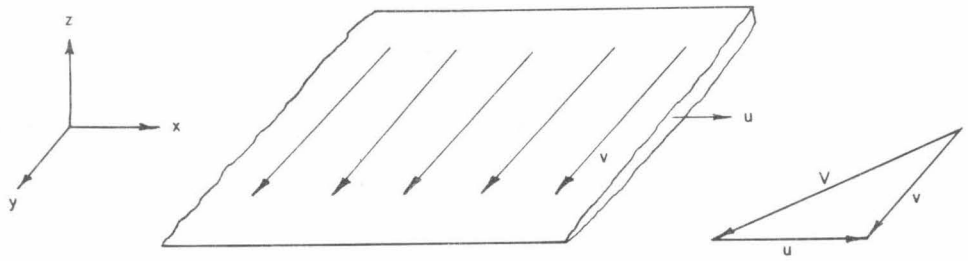

Fig. 19

The conditions in the boundary layer can be identified by use of a Reynolds number $R_x = Vx/\nu$, in which V is the relative velocity, x is the distance from the edge of the plate in the dire ction of the relative velocity, and ν is the kinematic viscosity of the fluid.

Similarity of stress conditions results when v/u and R_x are equal for two conditions of flow. In the experimental work, R_x for a given point and a given v/u varied somewhat due to the change in v. However, the variation was relatively small. The fact that C_D was the same function of the ratio of rotative speed to the speed of the approaching flow for all conditions for the hemispherical nose seems to follow from these considerations. They, however, do not take into account any change in the area of contact such as occurred.

A Reynolds number for flow about a rotating sphere is presented in reference 4. It is a modification of the form $R_x = Vx/\nu$ used for the flat plate. The relative velocity at a point is evaluated as the vector sum of the meridional and peripheral velocities based upon an inviscid fluid. The distance is evaluated in terms of the resultant relative path. The new form is $R_{R'} = R_x/\cos^2\phi$ in which $\phi = \tan^{-1} \omega r/1.5\ V_o$, ω is the angular velocity, r is the radius of the sphere and V_o is the approach velocity.

In addition to the above, the fluid about a rotating hemispherical nose is subjected to an acceleration normal to the axis of rotation of magnitude $r\omega^2$, where r is the local radius of the body and ω is the rotative speed. This will tend to produce a pressure gradient through the boundary layer and affect the pressure distribution. As seen in Fig. 20, the centrifugal acceleration a_r can be considered as composed of the elements a_n, an acceleration normal to the flow at the surface and a_s, parallel with the flow. The former component will tend to produce a pressure change through the boundary layer. The latter component will act to accelerate the fluid in the boundary layer.

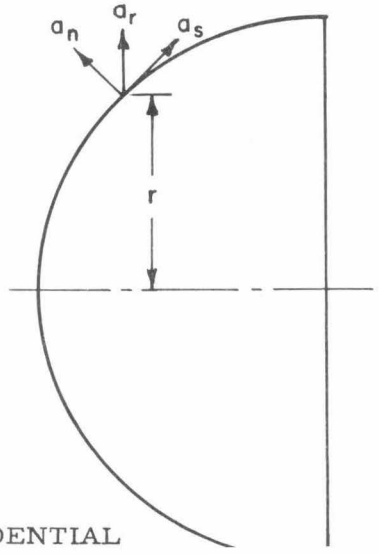

Fig. 20

As the fluid progresses along the hemisphere it is subjected to a tangential acceleration in planes normal to the axis of rotation because it is being brought into regions of increasing peripheral velocities due to its increasing distance from the axis of rotation. As a consequence its path and velocity at any point do not correspond to the values determined from simple superposition.

The shear stresses are proportional to the velocity gradient normal to the surface. Representing the shear stress by τ, the viscosity by μ, and the velocity gradient normal to the surface by du/dy. $\tau = \mu\, du/dy$.

The velocity gradient normal to the surface of a stationary disk which is normal to a flow is a relatively flat one which steepens from the center to the periphery. This implies the possibility of building up a relatively thick boundary layer on the surface of the disk when it is rotated. This indicates a small shear stress and little influence of the rotation upon the flow. This corresponds to observed results.

The velocity gradient normal to the surface of a stationary hemisphere whose axis is parallel to the direction of flow is relatively steep and the boundary layer is thin. This indicates a high shear stress. However, in cavity flow the area subjected to this stress is small. Rotation of the hemisphere about an axis parallel to the flow will change the velocity distribution in the boundary layer. It will also produce accelerations in planes normal to the axis of rotation. An expected consequence of these influences is a modification of the pressure distribution. The observed results can be interpreted in these terms. However, a factor to consider is the possible change of flow conditions due to increased Reynolds number.

EVALUATION

An uncertainty of unknown magnitude exists in the data. However, although it reflects on the precision of the results, indications are that it is too small to compromise the validity of the basic observations and measurements.

During these tests, readings were taken not only of the drag force but also of the cross-force and yawing-moment components. From the nature of the balance and symmetry of the test setup, at nominally zero yaw and pitch, it was expected that the cross-force component would produce a measure of the spin-decelerating moment and the yawing-moment component would register as zero. The actual results differed markedly from the predicted ones. A yawing moment which was a function of rotative speed and direction, and approach velocity, was observed. A cross force which was also a function of rotative speed and direction, and approach velocity, also occurred. The cross force, and seemingly the yawing moment, were not symmetrical in that not only the sign but the magnitude as well changed with direction of rotation. The yawing moment data showed considerable scatter.

Some general conclusions about the behavior of forces and moments with respect to direction of displacements can be drawn for a symmetrical body.[10] In this case, the test shape and shielding were nominally symmetrical about a vertical plane through the axis of the model. For such conditions a change in direction of rotation should not affect the magnitudes of any of the forces or moments. It should change the direction of cross force, spin decelerating moment and yawing moment but not of the drag force, lift force, or pitching moment. The behavior of the directions of the forces was in accordance with this principle. The fact that the cross-force and yawing-moment readings changed in absolute magnitude indicates the presence of asymmetry. The only asymmetry in the model with respect to the tunnel axis was a nose-up pitch of one minute of arc. Somewhat larger asymmetries existed in the shields.

The possibility of a pitching moment resulting from a component of the force producing the asymmetric yawing moment and cross force must be considered since it would influence the drag reading of the balance system used. It has been concluded that no significant pitching moment existed. This conclusion is based upon the fact that the change in drag with rotative speed was independent of the approach velocity, whereas both the cross force and yawing moment were significantly dependent upon approach velocity. The vertical component of a generalized interference force at the nose would have to have been an inverse function of the approach velocity, while the cross-force and yawing-moment component would have been a direct function to account for the results observed.

Visual observations indicated a change in the flow conditions at the nose with rotation. Such a change can be expected to produce a change in the drag force. It is known that such changes in flow conditions occur in the absence of interference caused by such items as struts and shielding.[9]

The experimental work was not carried further, nor were the anomalous effects of asymmetry investigated, because the test unit motor failed.

That the dye stripe painted on the nose for measuring rotative speed did influence the flow somewhat is indicated in Fig. 21. This occurred despite the thinness of the stripe. In this photograph, near the top of the cavity, is seen a glassy stripe on the cavity surface. This stripe is emanating from the dye stripe on the nose. The effects of the stripe are not considered significant in terms of the forces measured. It was observed that the flow pattern remained fixed with respect to the nose. No significant differences in measurements were observed whether the rotative speed was determined from observation of the dye stripe or the flow pattern without a stripe.

Since cavities whose diameters were a significant fraction of the diameter of the test section were formed under test conditions, some consideration must be given to the influence of walls upon the flow and the data. Although the wall effect has been evaluated analytically for the two-dimensional cavitation condition,[11] no similar investigation has yet been made of the three-dimensional case. However, it is understood that the case is now being analyzed.

Even though information for correcting cavitation data has not been developed, the proximity of the test conditions to certain limiting conditions can be determined. These limiting conditions are ascertained from considerations of energy, continuity and momentum, as discussed in Appendix II. A maximum possible value of the ratio of object diameter to tunnel diameter exists for each combination of drag coefficient and cavitation number. By comparing the actual ratio of object to tunnel diameter with the limiting ratio, the proximity of actual to limiting conditions is found.

For the hemispherical nose, a K of 0.30 and a C_D of 0.39, the limiting diameter ratio d/D is 0.29. The actual d/D is 2.375/14.0 = 0.17. The ratio of actual to critical is 0.17/0.29 = 0.59. It is believed that this ratio is small enough to indicate lack of measurable wall effects. For the truncated cone nose treated as a disk, C_D is 1.01, and K is 0.25. The critical d/D is 0.15. The actual d/D is 1.25/14.0 = 0.089. The ratio of actual to critical is 0.089/0.15 = 0.60. This is of the same order as for the hemispherical nose and assumed free of wall effects.

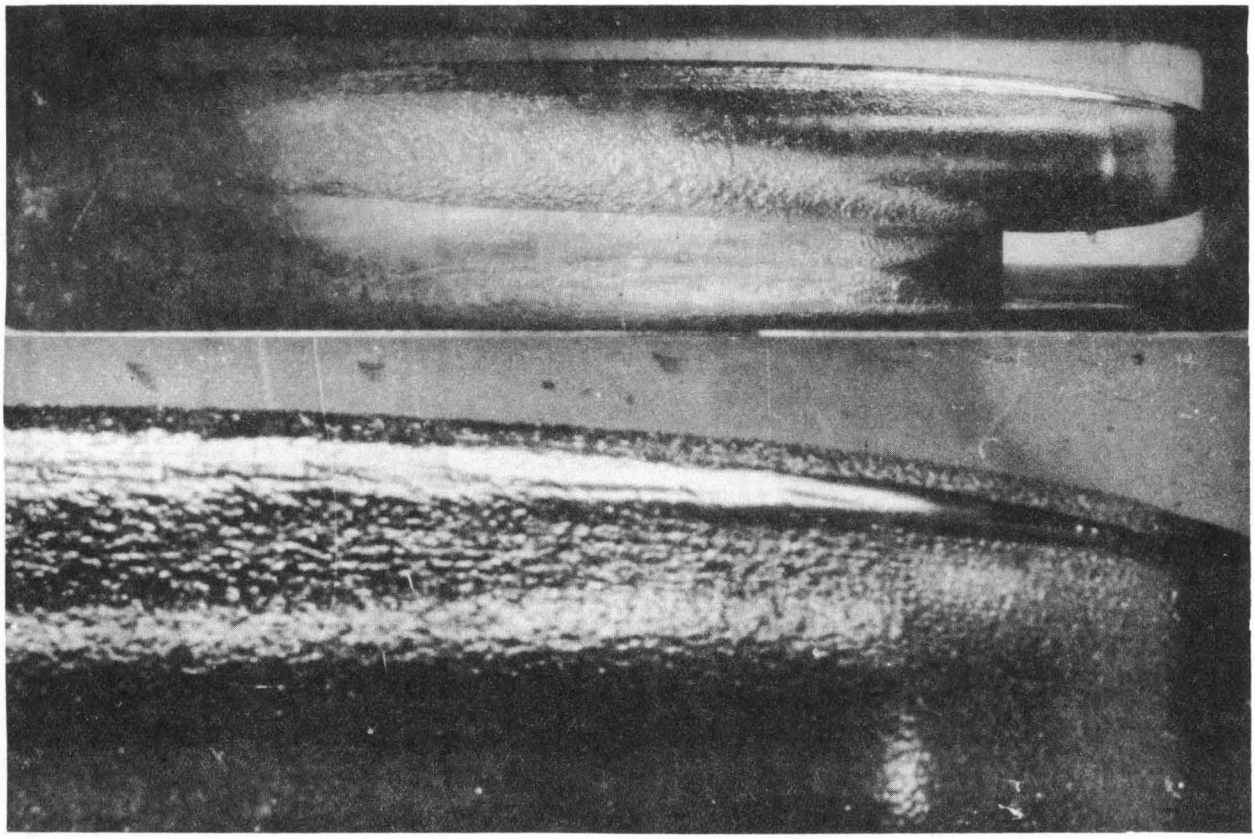

Fig. 21 - Stripe of Dye on Nose Produces Local Smoothing of Cavity Wall

V = 55 ft per sec

APPENDIX I

Summary of Data for Hemispherical Nose

Run	V ft/sec	N* rpm	D lbs	K
6	39.1	0	17.85	0.30
		+1800	17.97	0.30
		+3600	17.84	0.30
		+5400	16.38	0.29
		+7200	15.46	0.29
		+5400	16.12	0.29
		+3600	17.12	0.29
		+1800	17.93	0.29
7	54.7	+1800	35.29	0.29
		+7200	33.17	0.28
		0	36.06	0.30
		+1800	35.49	0.30
		+3600	34.81	0.29
		+5400	34.16	0.29
		+3600	34.54	0.29
		+7200	33.02	0.30
8	29.7	+1800	9.59	0.30
		+3600	9.64	0.30
		+5400	8.54	0.28
		+7200	7.54	0.24
		+6300	7.85	0.26
		+4500	8.91	0.28
10	54.8	0	35.74	0.29
		-1800	35.48	0.29
		-3600	34.96	0.29
		-7200	33.20	0.29
11	54.5	0	35.54	0.29
		-7200	32.27	0.29
		+7200	32.32	0.29
12	38.9	0	17.71	0.30
		-1800	17.56	0.29
		-3600	16.91	0.29
		-7200	14.89	0.27
13	39.1	-5400	15.74	0.28
		-7200	15.46	0.28
		-3600	17.03	0.28
		+7200	14.98	0.27
14	54.6	+5400	33.58	0.29
22	29.3	0	9.94	0.30
23	39.3	0	17.86	0.29
		-1800	17.63	0.29
		-3600	17.08	0.29
		-4500	16.68	0.29
		-5400	15.96	0.29

* + represents clockwise rotation looking upstream.

APPENDIX II

Limiting Conditions on Cavitation Studies in Closed-Section Circular Water Tunnels

THE CHART OF LIMITING SIZE RATIOS

Comparisons of conditions at which experiments in cavity flow are conducted with theoretical limiting conditions are aided by the use of the chart which is presented as Fig. 22. This chart facilitates determination of the maximum possible values of the ratio of the diameter of the test object to the channel diameter for any set of values of drag coefficient and cavitation number. Each maximum value of this ratio represents the theoretical limiting condition for operation for the given condition of cavitation number and drag coefficient.

To use the chart, enter it at the bottom with the experimental or assumed value of the cavitation number and proceed upward to intersect the curve, interpolated if necessary, corresponding to the related value of the drag coefficient. At this level proceed to the left margin to read the associated value of d/D, the limiting ratio of object diameter to channel diameter. From the known dimensions of the object and channel, determine the actual ratio of object diameter to channel diameter. Compare the actual ratio with the theoretical limiting ratio. If the values are close, consideration should be given to the effect of the finite size of the stream. If the actual ratio is considerably smaller than the limiting ratio, it is believed that the channel walls are producing no significant effect on the measured data.

The limitation on this method is that neither experimental nor theoretical information is available to indicate how close the actual ratio of diameters may approach the limiting ratio before the effect of the walls produces significant changes in the conditions being observed. However, until such information has been supplied to place the evaluation of wall effect on a sound basis, this method can serve to indicate how closely experimental conditions approach the theoretical limit. The actual ratio can be modified by changing the size of object or tunnel or both to keep it low.

DEVELOPMENT OF CHART OF LIMITING SIZE RATIOS

Relationship between Cavity Diameter and Channel Diameter

Application of the principles of conservation of energy and mass to flow about a cavity in a closed conduit shows that a maximum value of the ratio of cavity diameter to channel diameter or minimum value of the ratio of channel diameter to cavity diameter exists for each value of cavitation number. Consider the three-dimensional case of a body in cavity flow with an incompressible liquid of density ρ in an enclosed circular stream and coaxial with it, as indicated in Fig. 23. Apply Bernoulli's equation between a point sufficiently upstream to be essentially undisturbed, with velocity V_∞ and pressure p_∞, and a point in the liquid at the maximum cross section of the cavity, with velocity V_c and pressure p_c, and neglect friction losses

$$\rho \frac{V_\infty^2}{2} + p_\infty = \rho \frac{V_c^2}{2} + p_c$$

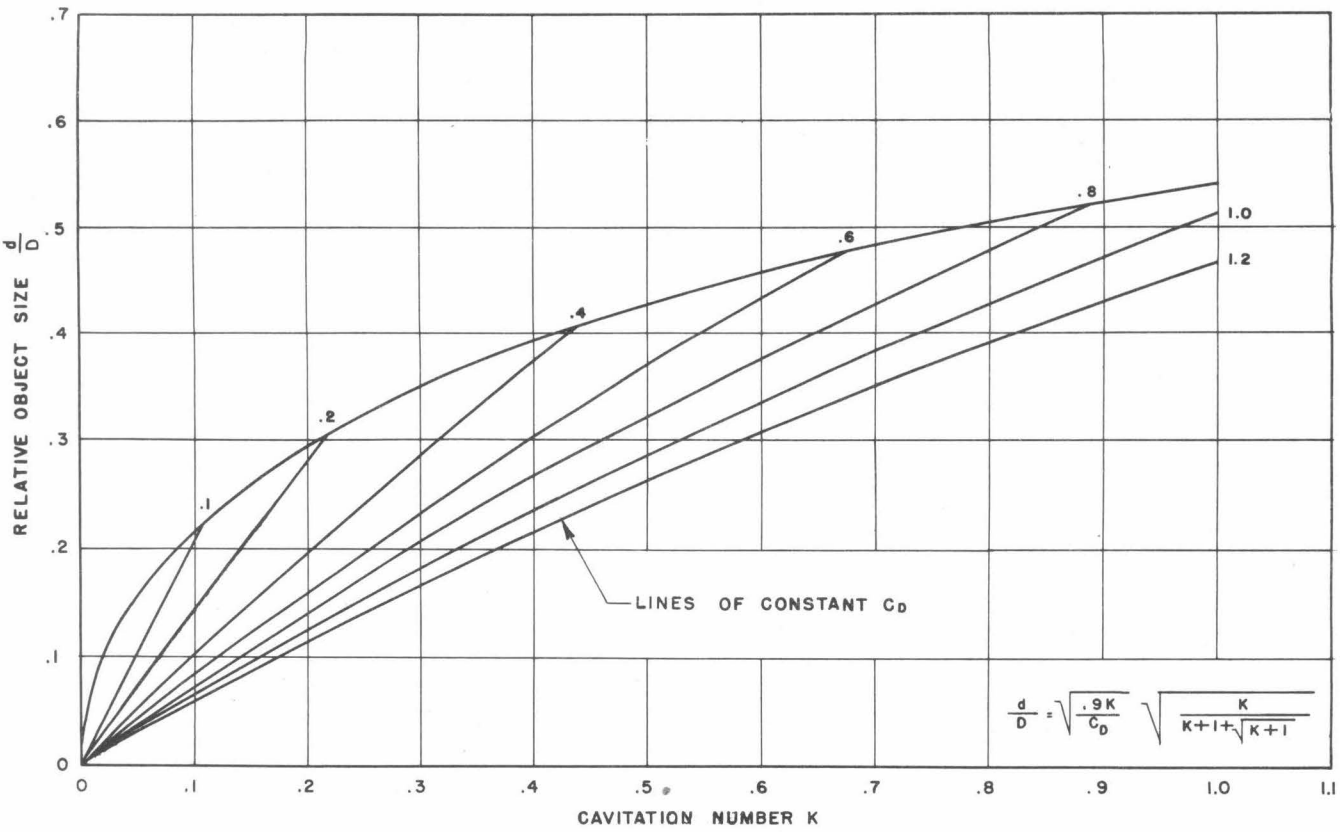

Fig. 22 - Chart for Determining the Limiting Ratio of Test Object Diameter to Closed Circular Test Channel Diameter for any Combination of Drag Coefficient and Cavitation Number

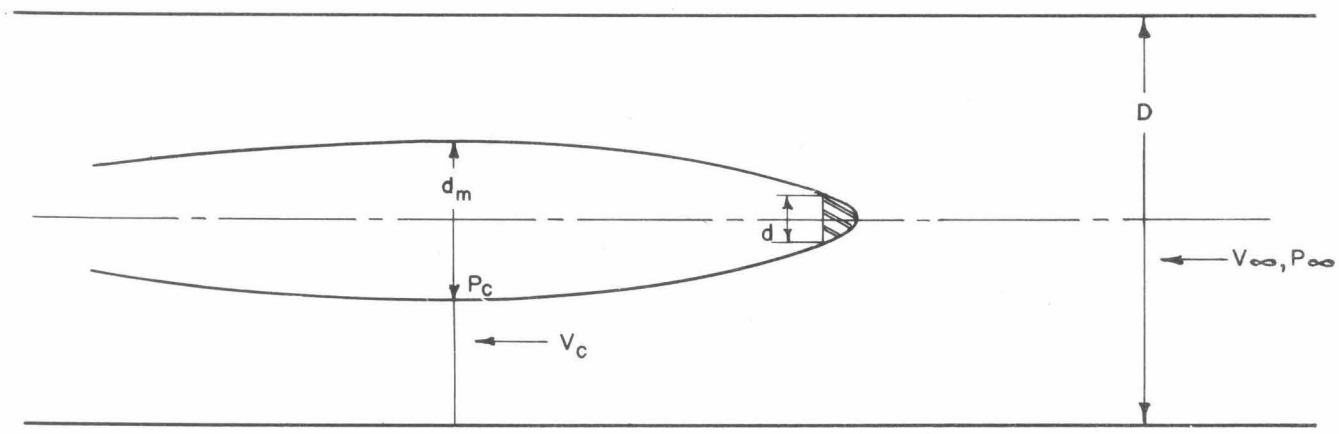

Fig. 23

The maximum velocity V_c for a given bubble diameter occurs when a minimum pressure exists uniformly across the channel cross section where the cavity diameter is a maximum. Because the curvature of streamlines along the bubble is convex outward from the axis of the channel, any pressure gradient which exists must be in the nature of an increase in pressure outward from the bubble to the tunnel wall. Thus, the minimum possible pressure is p_c the bubble pressure.

We identify the cavitation condition by the value of the cavitation parameter K

$$K = \frac{p_\infty - p_c}{\rho \frac{V_\infty^2}{2}}$$

in which

p_∞ = pressure of the undisturbed approaching liquid

p_c = pressure at the wall of the cavity

V_∞ = velocity of the undisturbed approaching liquid

A given value of the cavitation number K fixes the relationship among the upstream pressure, the bubble pressure, and the upstream velocity. The velocity corresponding to the minimum possible pressure p_c at the cross section of the maximum bubble diameter equals the maximum possible velocity under this condition. This must represent the condition of minimum possible cross section of flow or maximum possible cavity diameter.

Applying the principle of continuity for an incompressible fluid, and designating the tunnel diameter by D and the bubble diameter at the maximum cross section of the cavity by d_m

$$V_c = V_\infty \frac{D^2}{D^2 - d_m^2}$$

so that

$$p_\infty - p_c = \frac{\rho}{2} V_\infty^2 \left[\left(\frac{D^2}{D^2 - d_m^2} \right)^2 - 1 \right]$$

substituting

$$\frac{p_\infty - p_c}{\rho \frac{V_\infty^2}{2}} = K$$

$$K = \frac{2 \left(\frac{D}{d_m} \right)^2 - 1}{\left[\left(\frac{D}{d_m} \right)^2 - 1 \right]^2}$$

and, finally

$$\frac{D}{d_m} = \sqrt{\frac{K + 1 + \sqrt{K + 1}}{K}}$$

This shows that the ratio of the tunnel diameter to the bubble diameter at its maximum cross section is a function only of the cavitation number. A graphical representation of this equation is presented as Fig. 24.

The curve forms the ideal lower limit of the ratio D/d_m at which operation is possible for a given cavitation number. This results from the fact that, if the channel diameter, D, is considered fixed, the value of the bubble diameter used in the equation is the maximum physically possible for each value of K.

The limits of the curve are readily found by substituting the appropriate values of K in the equation for D/d_m. When $K = 0$, D/d_m goes to infinity. This emphasizes the fact, seen in the figure, that the channel size required for a given cavity size becomes much greater for low values of the cavitation number than for larger values. This limit can also be deduced from the form of the cavitation parameter. For a fixed value of approach velocity, the numerator is a measure of the potential energy available for conversion into kinetic energy. As the value of K decreases, the energy available for increasing the velocity of flow past the cavity also decreases. Thus a larger effective cross-sectional area of flow, or a larger D/d_m is required. When K goes to infinity, the ratio D/d_m reaches its lower limit of one, and the diameter of the bubble equals the diameter of the channel.

The actual limiting value of D/d_m for a given value of K must be larger than the ideal one obtained from the figure. This follows from the fact that a loss of head due to friction occurs between the upstream point at which p_∞ is measured and the point at which p_c is measured. The effective value of p_∞ is less than the ideal value. Thus the potential energy available for conversion into kinetic energy is less in the actual case than in the ideal case for the same cavitation number. As a result the effective value of K in the actual case for a given pressure difference and velocity is less than in the ideal case. Lower values of K require larger values of the ratio D/d_m.

A cavity of smaller than critical size can exist at a given condition of cavitation number and cavity pressure. This is the normal case. The bubble curvature is greater than in the limiting case so that a positive pressure gradient extends outward from cavity to the tunnel wall, and a lower average velocity exists to correspond to the greater average pressure and increased cross-sectional area.

Relation between Cavity Diameter and Object Diameter

From consideration of the change in momentum caused by the test object, it is found that a specific value of the ratio of cavity diameter at its maximum cross section to test object diameter exists for each combination of drag coefficient and cavitation number.

If a drag coefficient C_D' is defined on the basis of the maximum cross-sectional area of the bubble, it has been shown by Reichardt[6] that $C_D' = fK$ in which $f = 1 - 0.132\ K^{1/7}$. For the range of importance between $K = 0.1$ and 1.0, the value of f can be taken as 0.90 with an error of no more than 3 per cent. From the relationships

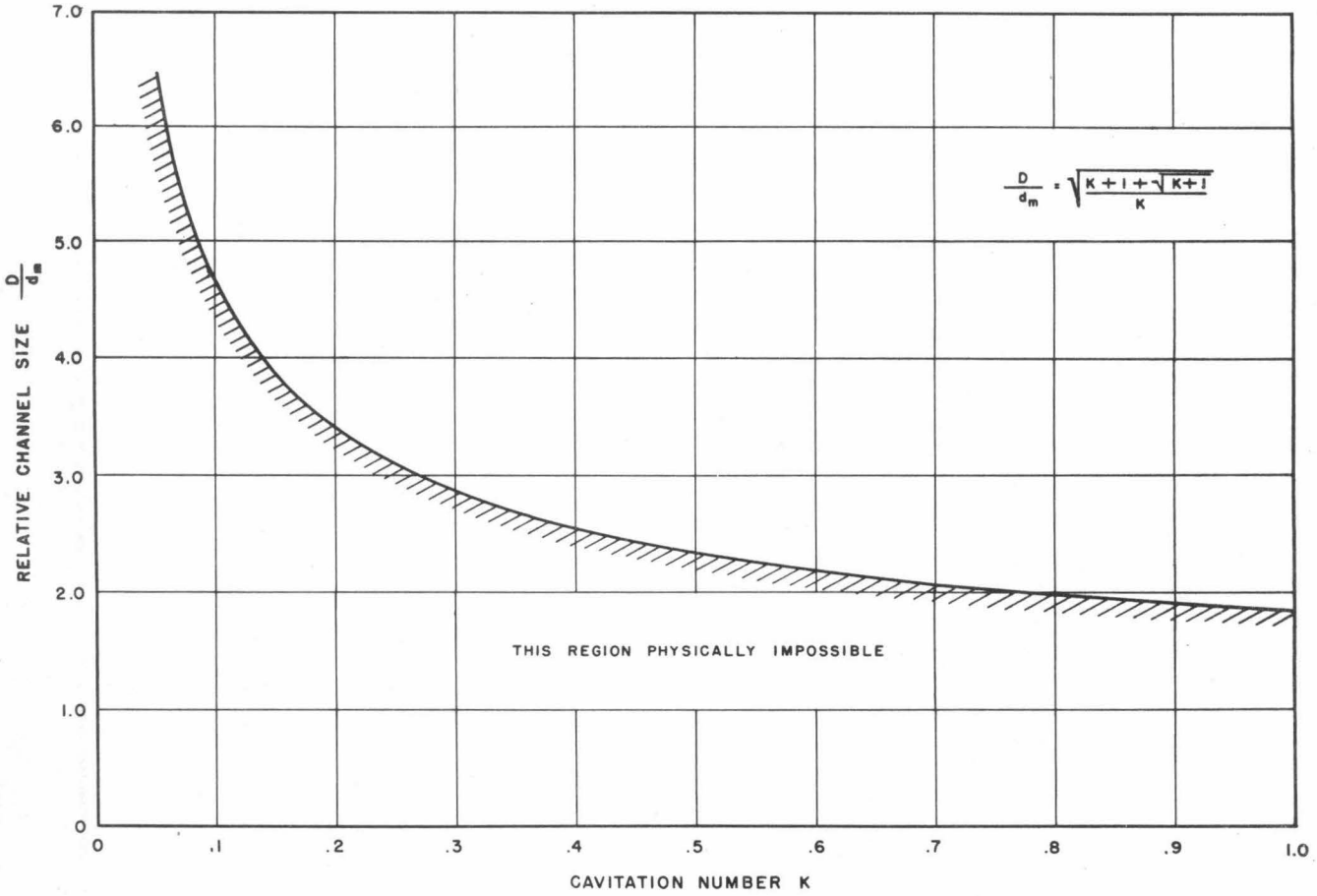

Fig. 24 - Limiting Ratio of Channel Diameter to Diameter of Cavity at Maximum Cross Section for any Cavitation Number

developed in reference 11, it is found that

$$\frac{d_m}{d} = \sqrt{\frac{C_D}{.9K}} \quad \text{in which}$$

d_m is the diameter of the cavity at its maximum cross section for the specified value of cavitation number K and d is the object diameter which is used in calculating C_D. This expression is presented graphically as Fig. 25 for a number of values of C_D.

The upper limit of the curves is infinity when K goes to zero. This emphasizes the rapid rate at which d_m/d increases at low values of K. Although the lower limit of the curves is zero when K becomes infinite, it is seen that all curves have been terminated at a value of d_m/d of one. This is equivalent to stating that the minimum possible cavity diameter equals the object diameter. This may not be strictly correct since the cavity on a sphere may form downstream from the equator thus having a diameter smaller than that of the sphere. However, the theoretical analysis assumes that there are no pressure forces on the object which give an upstream force component. This consideration requires that the cavity diameter be no smaller than the object diameter.

The points of intersection of the curves of constant C_D with the limiting condition of d_m/d do not appear to have any actual significance. In the ideal case, they should represent the conditions of K and C_D at which a cavity forms or collapses behind the object. Although no specific experiments have been made to investigate this, published data[8] indicate that this does not occur. Data for a 2-caliber ogive give a curve of rising C_D with K and a C_D of 0.26 at a K of 0.36. The chart predicts collapse when K is 0.29 for a C_D of 0.26.

The effect of the test section walls is to modify the pressure distribution in the stream about the cavity. From the analysis of the two-dimensional case it is found that this results in an upstream force. Thus the effect is equivalent to an increase in the drag and coefficient of drag of the body. From the expression for d_m/d, it is seen that an increase in drag coefficient increases the ratio d_m/d for a given value of K. Another way of looking at this is that the effect of walls is equivalent to decreasing the value of K for a given C_D, thus increasing the value of d_m/d.

Relationship between Channel Diameter and Object Diameter

By combining the factors which have been developed, the relationships between cavity and channel diameters and between cavity and object diameters, an expression for the interdependence of object size d and channel size D is obtained.

$$d/D = \sqrt{\frac{.9K}{C_D}} \sqrt{\frac{K}{K+1 + \sqrt{K+1}}}$$

Values of d/D as functions of K for several values of C_D have been presented as Fig. 22. For a given K and C_D condition, the chart gives the maximum value of d/D for which operation is ideally possible. It indicates the constricting effect of the walls.

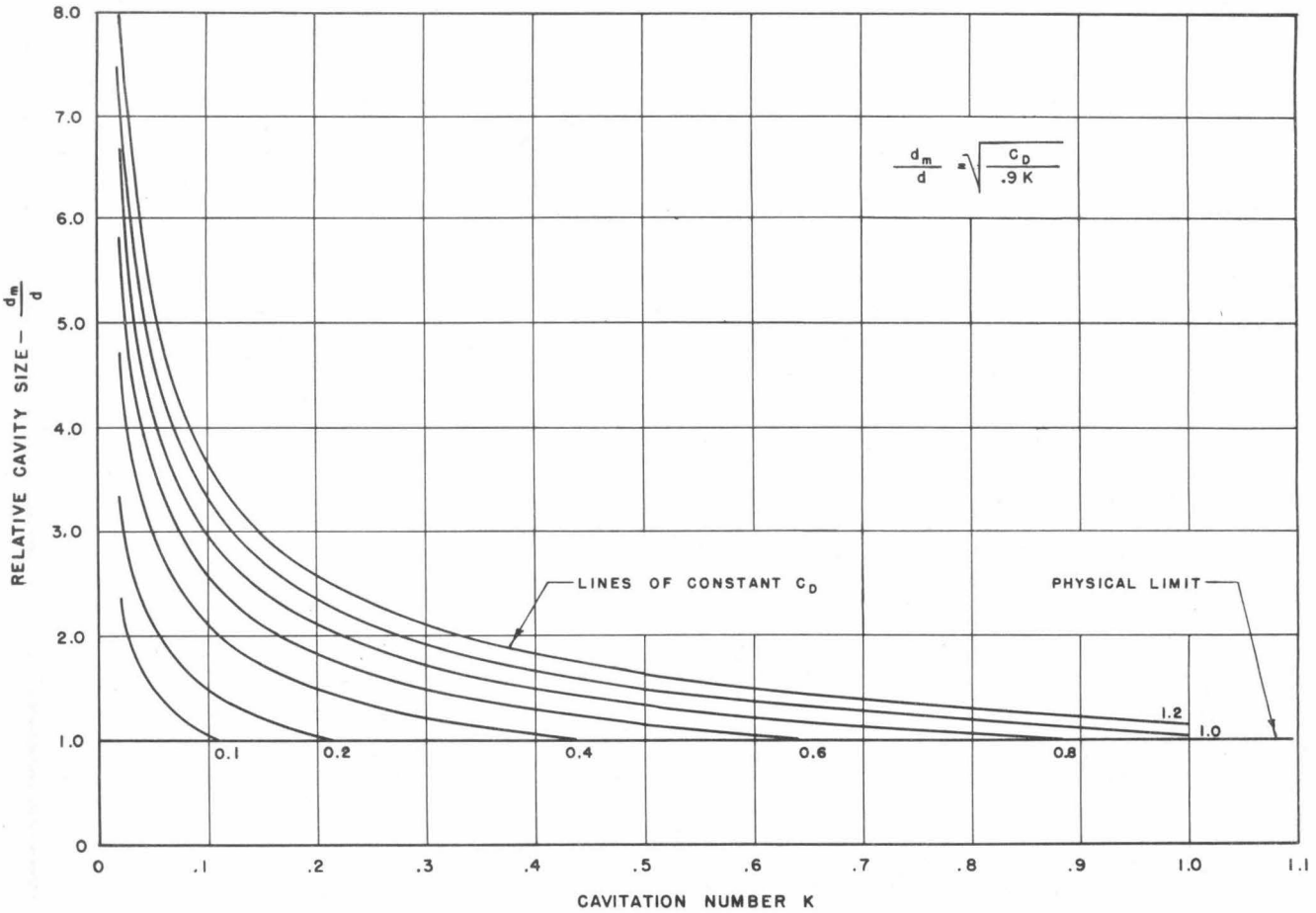

Fig. 25 - Ratio of Diameter of Cavity at its Maximum Cross Section to Diameter of Test Object for any Condition of Drag Coefficient and Cavitation Number

Since the effect of friction can be interpreted in terms of a decreased value of K, it is seen that the limiting relative object size d/D for a given C_D is less for a real liquid than for an ideal one. The walls modify the pressure distribution in the stream. This has been interpreted as being equivalent to an increase in the drag coefficient. This results in a larger relative cavity size for a given cavitation number. This also indicates a smaller limiting value of d/D than in the ideal case.

The upper limiting curve results when the condition that d_m/d is never less than one is applied. Since

$$d_m/d = \sqrt{\frac{C_D}{.9K}} = 1, \quad \text{the limiting condition is}$$

$$d/D = \sqrt{\frac{K}{K+1 + \sqrt{K+1}}}$$

With the information which has been developed, it is possible to determine the limiting ratio of object diameter to channel diameter for any value of K and C_D. The preliminary approach is to assume that, if under the conditions of actual operation, the value of the ratio of object to channel diameters is not close to the limiting one, there need be no fear of wall effects. On the other hand, if the ratios approach one another closely, wall effects may be playing a significant role. Unfortunately, neither theoretical nor experimental information as yet indicates how close the actual ratio can come to the theoretical ratio before wall effects must be considered.

BIBLIOGRAPHY

1 Daily, James W., "Hydrodynamic Forces Resulting from Cavitation on Underwater Bodies," Hydrodynamics Laboratory Report No. ND-31.2, July, 1945

2 Rouse, Hunter and McMown, John S., "Cavitation and Pressure Distribution," State University of Iowa, Studies in Engineering, Bulletin 32, 1948

3 Wieselsberger, C., "Uber den Luftwiderstand bei gleichzeitiger Rotation des Versuchskorpers," Physik.Zeitschr. XXVIII, pp. 84-88, 1927

4 Luthander, S. and Rydberg, A., "Experimentelle Untersuchung uber den Luftwiderstand bei einer um eine mit der Windrichtung parallele Achse rotierenden Kugel," Physik. Zeitschr., pp 522-558, 1935

5 Knapp, R. T.; Levy, J.; O'Neill, J. P.; and Brown, F. B., "The Hydrodynamics Laboratory of the California Institute of Technology," Trans. Am. Soc. of Mech. Engineers, Vol. 70, No. 5, pp. 437-457, July, 1948

6 Reichardt, H., "The Laws of Cavitation Bubbles at Axially Symmetrical Bodies in a Flow," Reports and Translation No. 766, Ministry of Aircraft Production, August 15, 1946. (Distributed by Office of Naval Research, Navy Dept., Washington, D. C.)

7 Plesset, M. S. and Shaffer, P. A., Jr., "Cavity Drag in Two and Three Dimensions," Journal of Applied Physics, Vol. 19, No. 10, pp 934-939, October, 1948

8 Eisenberg, P. and Pond, H. L., "Water Tunnel Investigations of Steady State Cavities," The David Taylor Model Basin, Navy Dept., Washington, D. C., Report No. 668, October, 1948

9 Wayland, Harold and White, Frank G., "Boundary Layer Effects on Spinning Spheres," Proceedings of the 1949 Heat Transfer and Fluid Mechanics Institute, The American Society of Mechanical Engineers

10 von Mises, R., "Theory of Flight," McGraw-Hill Book Co., Inc., 1st Ed., p. 572

11 Simmons, N., "The Geometry of Liquid Cavities with Especial Reference to Effects of Finite Extent of the Stream," Technical Report No. 17/48, Armaments Design Establishment, Ministry of Supply, Fort Halstead, Kent, August, 1948

DISTRIBUTION LIST

15	Office of Naval Research, Department of the Navy, Washington 25, D.C., Attn: Fluid Mech. Br. (Code 426)
1	Commanding Officer, Branch Office, U.S. Navy Office of Naval Research, 495 Summer Street, Boston 10, Massachusetts
1	Commanding Officer, Branch Office, U.S. Navy Office of Naval Research, 50 Church Street, New York 7, N.Y.
1	Commanding Officer, Branch Office, U.S. Navy Office of Naval Research, 844 North Rush Street, Chicago 11, Illinois
1	Commanding Officer, Branch Office, U.S. Navy Office of Naval Research, 801 Donahue Street, San Francisco 24, California
2	Commanding Officer, Branch Office, U.S. Navy Office of Naval Research, 1030 East Green Street, Pasadena 1, California
2	Assistant Naval Attache for Research, U.S. Navy Office of Naval Research, American Embassy, London, England, Navy 100, F.P.O., New York, N.Y.
1	Naval Research Laboratory, U.S. Navy Office of Naval Research, Washington 20, D.C., Attn: Librarian (Code 2021)
1	Executive Secretary, Research and Development Board, National Defense Building, Washington, D.C.
1	Bureau of Aeronautics, Department of the Navy, Washington 25, D.C. Attn: Aero and Hydro Branch (Code De3)
1	Bureau of Ordnance, Department of the Navy, Washington 25, D.C. Attn: Code Re2c
1	Bureau of Ordnance, Department of the Navy, Washington 25, D.C. Attn: Code Re3d
1	Bureau of Ordnance, Department of the Navy, Washington 25, D.C. Attn: Code Re6a
2	Bureau of Ordnance, Department of the Navy, Washington 25, D.C. Attn: Code Re9
5	Bureau of Ordnance, Department of the Navy, Washington 25, D.C. Attn: Code Ad3
1	Naval Ordnance Laboratory, U.S. Navy Bureau of Ordnance, White Oak, Silver Spring 19, Md., Attn: Dr. R. J. Seeger
3	Underwater Ordnance Division, Naval Ordnance Test Station, 3202 E. Foothill Blvd., Pasadena, California
1	Bureau of Ships, Department of the Navy, Washington 25, D.C. Attn: Research Division (Code 372)
3	David Taylor Model Basin, Department of the Navy, Washington 7, D.C., Attn: Hydromechanics Department
1	Department of the Army, General Staff, National Defense Building, Washington, D.C., Attn: Director of Research and Development
1	Army Chemical Center, Medical Division, Maryland. Attn: Dr. F. A. Odell
1	Ballistic Research Laboratories, Department of the Army, Aberdeen Proving Ground, Maryland. Attn: Mr. R. H. Kent
1	Director of Research, National Advisory Committee for Aeronautics, 1724 F. Street, N.W., Washington 25, D.C.
1	Director, Langley Aeronautical Laboratory, National Advisory Committee for Aeronautics, Langley Field, Virginia
1	Dr. J. H. Wayland, Division of Civil and Mechanical Eng. and Aeronautics, California Institute of Technology, Pasadena, California
1	Professor G. Birkhoff, Department of Mathematics, Harvard University, 576 Widener Library, Cambridge 38, Massachusetts

1 Dr. K. S. M. Davidson, Experimental Towing Tank, Stevens Institute of Technology, Hoboken, New Jersey.

1 Dr. J. H. McMillen, Naval Ordnance Laboratory, Naval Gun Factory, Washington 25, D.C.

1 Dr. F. A. Maxfield, Bureau of Ordnance, (Code Re6a), Department of the Navy, Washington 25, D.C.

1 Dr. A. Miller, Bureau of Ordnance (Code Re3d), Department of the Navy, Washington 25, D.C.

1 Dr. H. Rouse, Iowa Institute of Hydraulic Research, State University of Iowa, Iowa City, Iowa

1 Dr. J. V. Wehausen, Hydromechanics Department, David Taylor Model Basin, Department of the Navy, Washington, D.C.

2 Superintendent, U.S. Navy Postgraduate School, Annapolis, Maryland

2 Director, U.S. Naval Electronics Laboratory, Point Loma, San Diego, California

2 Research Analysis Group, National Research Council, 2101 Constitution Avenue, Washington, D.C.

2 Commanding Officer, Naval Torpedo Station, Newport, Rhode Island

2 Commander, Naval Ordnance Test Station, Inyokern, China Lake, California

2 Commander, Naval Ordnance Laboratory, White Oak, Silver Spring 19, Maryland

1 Director, Ordnance Research Laboratory, Pennsylvania State College, State College, Pennsylvania. Via: Development Contract Officer, Pennsylvania State College, State College, Pennsylvania

1 Worcester Polytechnic Institute Alden Hydraulic Laboratory, Worcester, Massachusetts. Attn: Prof. J. L. Hooper. Via: Inspector of Naval Material, Attn: Development Contract Section, 495 Summer Street, Boston 10, Massachusetts.

1 Inspector of Naval Material, Development Contract Section, 1206 South Santee Street, Los Angeles 15, California